LAWRENCE
LIVERMORE
NATIONAL
LABORATORY

LLNL-JRNL-430453

53Mn-53Cr and 26Al-26Mg Ages of a Feldspathic Lithology in Polymict Ureilites

C.A. Goodrich, I.D. Hutcheon, N.T. Kita, B.A. Cohen, K. Keil

May 4, 2010

Earth and Planetary Science Letters

Disclaimer

This document was prepared as an account of work sponsored by an agency of the United States government. Neither the United States government nor Lawrence Livermore National Security, LLC, nor any of their employees makes any warranty, expressed or implied, or assumes any legal liability or responsibility for the accuracy, completeness, or usefulness of any information, apparatus, product, or process disclosed, or represents that its use would not infringe privately owned rights. Reference herein to any specific commercial product, process, or service by trade name, trademark, manufacturer, or otherwise does not necessarily constitute or imply its endorsement, recommendation, or favoring by the United States government or Lawrence Livermore National Security, LLC. The views and opinions of authors expressed herein do not necessarily state or reflect those of the United States government or Lawrence Livermore National Security, LLC, and shall not be used for advertising or product endorsement purposes.

^{53}Mn-^{53}Cr and ^{26}Al-^{26}Mg Ages of a Feldspathic Lithology in Polymict Ureilites

[1]Cyrena Anne Goodrich

[2]Ian D. Hutcheon

[3]Noriko T. Kita

[4]Gary R. Huss

[5]Barbara Anne Cohen

[4]Klaus Keil

[1]Planetary Science Institute
1700 E. Ft. Lowell Drive
Tucson, AZ 85719-2395 USA
cyrena@vermontel.net
cgoodrich@psi.edu
Telephone: 802-875-1509
FAX: 520-622-8060
(correspondence author)

[2] Glenn T. Seaborg Institute,
Lawrence Livermore National Laboratory,
Livermore, CA 94551 USA

[3]Department of Geoscience
University of Wisconsin-Madison
1215 W. Dayton Street,
Madison, WI 53706-1692, USA

[4]Hawaii Institute of Geophysics and Planetology
University of Hawaii at Manoa
Honolulu, HI 96822 USA

[5]NASA Marshall Space Flight Center
Huntsville, AL 35812 USA

Submitted to *Earth and Planetary Science Letters*, December 2009.

Revised, April 2010.

Abstract

We report ^{53}Mn-^{53}Cr and ^{26}Al-^{26}Mg isotopic data, obtained by in-situ SIMS analysis, for feldspathic clasts in polymict ureilites DaG 319 and DaG 165. The analyzed clasts belong to the "albitic lithology," the most abundant population of indigenous feldspathic materials in polymict ureilites, and are highly-fractionated igneous assemblages of albitic plagioclase, Fe-rich pyroxenes, phosphates, ilmenite, silica, and Fe(Mn, K, P, Ti)-enriched glass. Glass in DaG 165 clast 19 has extremely high and variable ^{55}Mn/^{52}Cr ratios (500-58,000) and shows correlated ^{53}Cr excesses up to ~1,500‰, clearly indicating the presence of live ^{53}Mn at the time of formation. The slope of the well-correlated isochron defined by glass and pyroxenes from this clast corresponds to (^{53}Mn/^{55}Mn)= (2.84±0.10)×10^{-6} (2σ). Data for less ^{55}Mn/^{52}Cr-enriched glasses from DaG 319 clast B1, as well as phosphates from several other clasts, are consistent with this isochron. The ^{53}Mn/^{55}Mn ratio obtained from the isochron implies that these clasts are 0.70±0.18 Ma younger than the D'Orbigny angrite, corresponding to the absolute age of 4563.72±0.22 Ma. Plagioclase in DaG 319 clast B1 has a fairly constant ^{27}Al/^{24}Mg ratio of ~900 and shows resolvable ^{26}Mg excesses of ~2‰. The slope of the isochron defined by pyroxene and plagioclase in this clast is (3.0±1.1)×10^{-7} (2σ), corresponding to a time difference of 5.4 (-0.3/+0.5) Ma after CAI (assuming the canonical initial ^{26}Al/^{27}Al ratio of 5×10^{-5}) and an age 0.5 (-0.3/+0.5) Ma younger than D'Orbigny. Its absolute age (relative to D'Orbigny) is 4563.9 (+0.4/-0.5) Ma, in agreement with the ^{53}Mn-^{53}Cr age from clast 19.

These data provide the first high-precision age date, ~5.4 Ma after CAI, for ureilites, giving a minimum estimate for the age of differentiation of their parent asteroid. Interpretation of this age for the thermal and physical history of that asteroid depends on a number of currently unknown or model-dependent parameters, including its size, bulk composition, and oxidation state, and the petrologic relationship between the feldspathic clasts and main group ureilites.

Key Words: ureilite, early solar system chronology, Mn-Cr isotopes, Al-Mg isotopes

1. Introduction

Chronological studies of asteroidally-derived differentiated meteorites indicate that planetary bodies in our solar system accreted and were heated to the point of melting very shortly after formation of the first solids (CAIs, for which the oldest absolute ages of 4567-4569 Ma have been reported; Amelin et al., 2002, 2009; Bouvier and Wadhwa, 2009). This has been known for a long time based on the long-lived ^{87}Rb-^{87}Sr, ^{147}Sm-^{143}Nd and U-Th-Pb chronometers, with the most precise absolute ages being given by the Pb-Pb system (e.g. Amelin, 2008a,b; Baker et al., 2005; Lugmair and Galer, 1992; Tatsumoto et al., 1973; Wadhwa et al., 2009; Wasserburg et al., 1977). The application of relative chronometers based on short-lived radionuclides such as ^{53}Mn-^{53}Cr and ^{26}Al-^{26}Mg has resulted in even greater time resolution (≤1 Ma) among ancient samples, and when anchored to absolute ages can provide a very detailed timescale for the early solar system (e.g. Lugmair and Shukolyukov, 1998, 2001; Spivak-Birndorf et al., 2009; Wadhwa et al., 2006, 2009). The majority of work on the timing of early differentiation has focused on two groups of basaltic meteorites – angrites and non-cumulate eucrites. In this paper, we report the first high precision age dates obtained from ^{53}Mn-^{53}Cr and ^{26}Al-^{26}Mg chronometry for another major group of achondritic meteorites, the ureilites. Preliminary results were reported in Goodrich et al. (2002) and Kita et al. (2007).

Unlike eucrites and angrites, which represent the melts produced during differentiation of their parent bodies, main group ureilites are ultramafic rocks believed to represent mantle residues. The majority are coarse-grained (mm-sized), highly-equilibrated assemblages of olivine + low-Ca pyroxene, with accessory carbon phases, metal, sulfides, and phosphides (Goodrich, 1992; Mittlefehldt et al., 1998). Although early workers interpreted them as cumulates (Berkley et al., 1976, 1980; Berkley and Jones, 1982; Goodrich et al., 1987), various lines of evidence now indicate that they are residues of ~25-30% partial melting (Goodrich, 1999; Goodrich and Delaney, 2000; Goodrich et al., 2007; Scott et al., 1993; Spitz and Boynton, 1991; Warren and Kallemeyn, 1992). A number of their characteristics, however, are difficult to explain in a normal igneous fractionation model. These include: 1) a large range of olivine Fo (~75-95) at near-constant Mn/Mg ratio, which indicates that they are related to one another principally by various degrees of reduction rather than various degrees of melting (Goodrich and Delaney, 2000; Goodrich et al., 1987; Mittlefehldt, 1986); 2) the dominance of high-Wo (~6-14) pigeonite over orthopyroxene, which is inconsistent with single-stage melting of chondritic materials (Goodrich, 1999; Goodrich et al., 2007); 3) oxygen-isotopic compositions that show a chondritic (i.e. slope ~1) trend, rather than a mass-dependent fractionation (slope ~1/2) trend, on a δ^{17}O-δ^{18}O diagram (Clayton and Mayeda, 1988; 1996); 4) near-chondritic abundances of

"planetary type" noble gases (Göbel et al., 1978); and 5) near-chondritic abundances of siderophile elements. Thus, ureilites have characteristics of both highly fractionated and very primitive meteorites (Goodrich, 1992; Mittlefehldt et al., 1998). One model that has been extensively discussed (Berkley and Jones, 1982; Goodrich et al., 1987, 2007; Singletary and Grove, 2003; Sinha et al., 1997; Walker and Grove, 1993; Warren and Kallemeyn, 1992; Wilson et al., 2008) is that carbon redox control ("smelting") might explain many of these characteristics and reconcile high degrees of melting with preservation of certain primitive features. However, even in this model siderophile elements are problematic (Mittlefehldt et al., 2005; Van Orman et al., 2009; Warren and Huber, 2006; Warren et al., 2006). The petrogenesis of ureilites remains unclear, and it is difficult to place them on any scale of degree of differentiation in the early solar system (Weisberg et al., 2006).

1.1. Previous Age Data for Main Group Ureilites

Data from long-lived radionuclide systems indicate that ureilite formation ages are very old. The most precise ages come from U-Th-Pb systematics, although the highly depleted nature of these rocks make it difficult to remove effects of terrestrial Pb contamination (Torigoye-Kita et al., 1995a,b). From MET 78008, an augite-bearing ureilite with exceptionally high abundances of incompatible trace elements, Torigoye-Kita et al. (1995b) obtained a Pb-Pb isochron age of 4563±21 Ma (using three pyroxene-rich acid-leached residues) and a U-Pb age of 4563±6 Ma with initial Pb only slightly evolved from Canyon Diablo Troilite (Tatsumoto et al., 1973).

Data for ^{147}Sm-^{143}Nd systematics also indicate old formation ages, but are complicated by the presence of a cryptic LREE-enriched component of uncertain origin (Boynton et al., 1976; Goodrich and Lugmair, 1995; Guan and Crozaz, 1995; Spitz and Boynton, 1991; Spitz et al., 1988). Samples that contain significant amounts of this component (Goodrich and Lugmair, 1995; Goodrich et al., 1991; Torigoye-Kita et al., 1995a) form a ^{143}Nd/^{144}Nd–^{147}Sm/^{144}Nd line with a slope corresponding to an age of 3.79±0.05 Ga and an initital ^{143}Nd/^{144}Nd ratio of 0.50938±4 (ε_{Nd} = +33.5). However, samples that contain little of it, including whole-rock samples of MET 78008, ALH 82130 and PCA 82506, have model (CHUR) ages close to 4.55 Ga (Goodrich et al., 1991; Takahashi and Masuda, 1990). In addition, acid leached residues of handpicked augite from MET 78008 give a model age of 4.57±0.03 Ga and excess ^{142}Nd at a level consistent with formation at ~4.56 Ga (Torigoye-Kita et al., 1995b). Thus, although the interpretation of the 3.79 Ga "age" is controversial (Goodrich et al.,1995; Torigoye-Kita et al., 1995c), it is clear that the igneous age of all analyzed ureilites is close to 4.56 Ga.

All ^{87}Rb-^{87}Sr isotopic data obtained for ureilites (Goodrich et al., 1991; Takahashi and Masuda, 1990) show disturbance and provide no meaningful age information. The ^{187}Re-^{187}Os isotopic system has also been disturbed. Analyses of 22 whole-rock samples show open system behavior of Re, and give no age information (Rankenburg et al., 2007). Nevertheless, two samples that are falls (Novo Urei and Jalanash) have Re-Os isotopic compositions similar to those of carbonaceous chondrites and plot close to a 4558 Ma $^{187}Os/^{188}Os$-$^{187}Re/^{188}Os$ reference line (Rankenburg et al., 2007).

Two short-lived radionuclide chronometers have been applied to the main group ureilites. Data from the ^{182}Hf-^{182}W system for eight ureilites (Lee et al., 2003, 2005) all show ^{182}W deficits relative to chondrites, indicating at least partial metal/silicate segregation within 1-2 Ma of formation of the solar system. In contrast, ^{53}Mn-^{53}Cr data for leachates and residues of various fractions from Kenna and LEW 85440 form a horizontal $^{53}Cr/^{52}Cr$-$^{55}Mn/^{52}Cr$ trend, indicating that Cr isotopes in these meteorites equilibrated after all ^{53}Mn ($t_{1/2}$ = 3.7 Ma) had decayed (Shukolyukov and Lugmair, 2006).

In summary, chronological studies of main group ureilites indicate that they are very old, but provide no resolution relative to other groups of meteorites or distinction of the various processes involved in differentiation on the ureilite parent asteroid.

1.2. Feldpathic Lithologies in Polymict Ureilites

There are no basaltic ureilites, and thus the only petrologic information we have about the melts that were complementary to these mantle rocks is what can be deduced from the polymict ureilites, which are regolith breccias. Although dominated by fragmented materials similar to main group ureilites, these samples contain a few percent feldspathic material in the form of small (<500 μm) lithic and mineral clasts (Cohen et al., 2004; Downes et al., 2008; Goodrich et al., 2004; Ikeda and Prinz, 2001; Ikeda et al., 2000; Kita et al., 2004; Prinz et al., 1988). At least nine different types of feldspathic (containing plagioclase or glass of feldspar-like composition) clasts have been distinguished, but only four are likely to be both pristine (i.e. not melted, mixed, or reduced by shock) and indigenous (as determined by O-isotopes; Kita et al., 2004, 2006) to the ureilite parent asteroid. Of these, by far the most common is a population of lithic and mineral clasts that was named “the albitic lithology” by Cohen et al. (2004), and includes “group 3” clasts of Prinz et al. (1988) and most “type C1” clasts of Ikeda et al. (2000) and Ikeda and Prinz (2001). These clasts appear to represent a distinct igneous lithology, which is characterized by a

phase assemblage of albitic (An ~0-28) plagioclase, pyroxenes of ferroan (Fe/Mg up to 2.1) intermediate- to high-Wo compositions (Fig. 1), phosphates (Cl-apatite and whitlockite), ilmenite, a silica phase and glassy mesostasis rich in FeO (molar Fe/Mg up to 20), MnO, K_2O, P_2O_5 and TiO_2. Its overall texture is plagioclase-porphyritic, with groundmass areas consisting of smaller plagioclase laths, sub/anhedral to skeletal pyroxenes, and mesostasis (Cohen et al., 2004). Although only a few of the clasts identified as belonging to this lithology show this complete phase assemblage and overall texture, derivation from a common melt is supported by extensive normal fractional crystallization trends of Fe/Mg vs. Fe/Mn in pyroxenes and Fe/Mg vs. An in coexisting plagioclase (Fig. 2).

The only chronological information available for polymict ureilites is what has been published in a few abstracts (including our own preliminary reports; Goodrich et al., 2002; Kita et al., 2007). Davis et al. (1988) measured Mg isotopic compositions in a few plagioclase grains (of unspecified composition) in the North Haig polymict ureilite. Their results produced only an upper limit on the initial $^{26}Al/^{27}Al$ ratio ($<1x10^{-6}$), corresponding to an upper age limit of ~3.5 Ma after CAI. However, using improved analytical methods, Kita et al. (2003) found that plagioclase from 10 clasts in DaG 319 (6 of which belong to the albitic lithology) showed excess ^{26}Mg correlated with $^{27}Al/^{24}Mg$ ratio, with a slope of $\sim 4x10^{-7}$ corresponding to ~5 Ma after CAI. In addition, Kita et al. (2002) obtained a Pb-Pb isochron age of 4559±29 Ma for an apatite grain in one clast in DaG 319 belonging to the albitic lithology (Kita et al., 2002).

In this work we investigated ^{53}Mn-^{53}Cr and ^{26}Al-^{26}Mg isotopic systematics in four clasts belonging to the albitic lithology – clast B1 from DaG 319 and clasts 19, 9 and 20 from DaG 165. All of these were included in the oxygen isotopic study of Kita et al. (2006) and confirmed to be indigenous to the ureilite parent body. The goal of this investigation was to obtain high-precision age data (comparable to that available for angrites and eucrites) for the dominant silicate melt component in ureilites, in order to elucidate the differentiation history of the ureilite parent body and more generally increase our knowledge of the timing of differentiation in the early solar system.

2. Analytical Techniques

2.1. Scanning electron microscopy and electron microprobe analysis

Back-scattered electron images (BEI) were obtained using the JEOL JSM-LV5900 scanning electron microscope at Hawaii Institute of Geophysics and Planetology (HIGP). Mineral compositional data were obtained using the CAMECA SX50 electron microprobe at HIGP. Analytical conditions are described in Cohen et al. (2004).

2.2. Secondary Ion Mass Spectrometry (SIMS), Mg-Al

Al-Mg isotope analyses were carried out in three laboratories –Lawrence Livermore National Laboratories (LLNL), Arizona State University (ASU) and the Geological Survey of Japan (GSJ).

2.2.1. LLNL SIMS

Magnesium isotope ratios and $^{27}Al/^{24}Mg$ ratios were measured at LLNL using a modified Cameca ims-3f ion microprobe. An $^{16}O^-$ primary ion beam with 0.1 to 2 nA current and 14.5 keV impact energy was focused into a spot of ~3 to 10 micron diameter. For the analyses of standards, the primary ion current was adjusted to keep the intensity of $^{24}Mg^+$ below 2.5×10^5 sec^{-1} to minimize the effect of counting system dead time corrections. The effective dead time was determined at regular intervals using Ti isotope measurements (Fahey et al, 1987) and remained stable at a value of 25 ± 2 nsec throughout the study. For analyses of minerals and glasses with high Al/Mg ratios, the $^{27}Al^+$ intensity was measured by electrostatically deflecting the secondary ion beam into an off-axis Faraday cup. The efficiency of the electron multiplier was calibrated against the Faraday cup using measurements of $^{27}Al^+$ in metal and mineral standards. Data were acquired using a 400 micron diameter contrast aperture with the mass spectrometer tuned to achieve a mass resolving power of 3000, sufficient to resolve hydride and Ca^{++} interferences. A field aperture inserted into the sample image plane allowed only secondary ions arising from a 30 micron diameter area centered around the point of primary ion beam impact to enter the mass spectrometer. Isotope measurements were carried out in peak jumping mode, through the mass sequence 23.8, 24, 25, 26 and 27; each analysis consisted of 60 to 300 cycles grouped into blocks of 10 cycles. Sample charging was monitored by measuring the energy distribution of $^{24}Mg^+$ at regular intervals during each analysis and, as needed, adjusting the sample high voltage to maintain the maximum in the energy distribution at a value of -17V relative to the voltage at which the intensity fell to 10% of its maximum value. The accuracy and reproducibility of the Mg isotope measurements was evaluated using glasses and minerals with terrestrial isotope composition and a set of anorthite glasses labeled with ^{25}Mg (Armstrong et al., 1982; McKeegan et al., 1985). Terrestrial standards included both Mg-rich phases (Burma spinel, Dekalb diopside, San Carlos olivine, fassaite glass), as well as samples with Al/Mg >100 (plagioclase glass, Lake County labradorite and Miakejima anorthite). The precision and accuracy in the measured $\delta^{26}Mg$ values are limited by ion counting statistics and lie between 1-3‰ (2σ), even in Mg-poor samples containing <0.05 wt.% Mg.

2.2.2. ASU SIMS

Magnesium isotope ratios and $^{27}Al/^{24}Mg$ ratios were measured at ASU using a Cameca ims-6f ion microprobe. The procedure was similar to that used at LLNL, except as noted. An O^- primary ion beam of 2-3 nA (4-5 microns) was used for plagioclase, while a 0.3 nA (1-2 microns) beam was used on high-Mg phases. The mass spectrometer of the ims-6f operates at +10 keV, giving an impact energy of 22.5 keV. The mass spectrometer was tuned to achieve a mass resolving power of ~3400, more than enough to resolve all interferences. An imaged field of ~35 microns was used to increase the number of secondary ions reaching the detectors. The effective dead time of the counting system was determined to be 32.5±2 nsec from measurements of Ti isotopes (Fahey et al., 1987). For plagioclase standards and plagioclase in the sample, the $^{24}Mg^+$ intensity was below 1 x 10^5 sec^{-1}, but for high-Mg phases, the $^{24}Mg^+$ count rate was ~8 x 10^5 sec^{-1}. Standards were Burma Spinel and Lake County Labradorite.

2.2.3. GSJ SIMS

Magnesium isotope ratios and $^{27}Al/^{24}Mg$ ratios were measured at the Geological Survey of Japan (GSJ) using a Cameca ims-1270 ion microprobe. The analytical conditions are similar to those described above, except as noted (Kita et al. 2000). An O_2^- primary ion beam was used instead of O^- for better ionization efficiency. The beam was shaped in Köhler illumination mode to ~12μm in diameter and the beam current was 0.3-0.4 nA. The dead time of the ion counting detector was determined to be 50-55 nsec from measurements of a plagioclase glass standard. The secondary $^{24}Mg^+$ ion intensities were ~2×10^4 cps for plagioclase in DaG-319 clast B1, so the uncertainty of the dead time correction (~5ns) does not contribute more than 0.1‰ of the sample analyses. Between 100 and 250 cycles were used for sample and standard depending on the count rate of the analyses. The measured $^{27}Al/^{24}Mg$ ratio was calibrated by using a plagioclase standard with known Al and Mg contents.

2.2.4. Reporting of data

Measuring the intrinsic mass-dependent Mg isotope fractionation of minerals in polymict ureilite clasts was not an objective of this study. Non-mass dependent variations in the $^{26}Mg/^{24}Mg$ ratio, expressed as $\delta^{26}Mg$ in permil (‰), were determined using a linear law to correct for both instrumental and any intrinsic mass-dependent fractionation:

$$\delta^{26}Mg = \Delta^{26}Mg - 2\times\Delta^{25}Mg,$$

where

$$\Delta^{i}\mathrm{Mg\ (permil)} = [\{(^{i}\mathrm{Mg}/^{24}\mathrm{Mg})_{meas} / (^{i}\mathrm{Mg}/^{26}\mathrm{Mg})_{ref}\} - 1]\times 1000;\ (i = 25, 26).$$

Reference values for $^{25}Mg/^{24}Mg$ and $^{26}Mg/^{24}Mg$ are 0.12663 and 0.13932, respectively (Catanzaro et al., 1966). The $^{27}Al/^{24}Mg$ ratios for the different minerals were determined from the measured ion ratios using appropriate sensitivity factors determined from analyses of terrestrial standards. All uncertainties are 2 standard deviations (2σ) and include the propagated error from the reproducibility of Mg isotope standards.

2.3. SIMS Analysis: Mn-Cr

Cr isotope ratios and $^{55}Mn/^{52}Cr$ ratios were measured at LLNL using a modified Cameca ims-3f ion microprobe. The procedure was similar to that used for Mg isotopes, except as noted. The mass spectrometer was tuned to achieve a mass resolving power of ~3500. As this resolution is insufficient to separate completely $^{53}Cr^{+}$ from $^{52}CrH^{+}$, the intensity of $^{53}Cr^{+}$ was not measured on peak center but rather ~2 millimass units (mamu) to the low mass side of the $^{53}Cr^{+}$ peak centroid. This protocol ensured that the contribution of $^{52}CrH^{+}$ to the measured $^{53}Cr^{+}$ intensity was insignificant, i.e., $^{53}Cr^{+}/^{52}CrH^{+}$ of < 0.001. Isotope measurements were carried out in peak jumping mode, through the mass sequence 49.8, 50, 52, 53, and 55; each analysis consisted of 60 to 300 cycles grouped into blocks of 10 or 20 cycles. Sample charging was monitored by measuring the energy distribution of $^{55}Mn^{+}$ at regular intervals during each analysis and, as needed, adjusting the sample high voltage to maintain the maximum in the energy distribution at a value of -19V relative to the voltage at which the intensity fell to 10% of its maximum value. The accuracy and reproducibility of the Cr isotope measurements were evaluated using Cr metal and natural and synthetic minerals with terrestrial isotope composition. Isotope standards included Cr-diopside, chromite, San Carlos and N-1 olivines, and a series of synthetic pyraphosphate minerals with Mn/Cr of 10 to 100.

Cr isotope ratios for the standards were corrected for mass-dependent fractionation using an exponential law after normalizing to $^{50}Cr/^{52}Cr = 0.051859$. Due to its very low intensity, $^{50}Cr^{+}$ was not monitored during the analyses of the DaG 319 samples. Rather, we assessed the overall variation in $^{50}Cr^{+}/^{52}Cr^{+}$ among the suite of silicate standards (~5‰) and included a term carrying a 5‰ relative uncertainty in the calculation of the propagated uncertainty for $^{53}Cr/^{52}Cr$. Variations in $^{53}Cr/^{52}Cr$ ratios are reported as $\delta^{53}Cr$ (‰) relative to the terrestrial ratio of 0.113589. Recent studies at LLNL and elsewhere (McKibbin et al., 2008; Sugiura et al., 2009) have indicated that the relative ionization efficiency for Mn and Cr is significantly affected by major element composition of the host

phase. We determined the relative sensitivity factor for calculating atomic Mn/Cr ratios from Mn^+/Cr^+ ion ratios by examining a series of 11 silicate glass and mineral samples with SiO_2 contents of 40-71 wt.% and FeO contents of 0.05-20 wt.% (Matzel et al., 2009). The RSF used for the DaG 165 and DaG 319 glasses is 1.121±0.056(2σ).

3. Results

3.1. Petrography and Mineral Compositions

Clast B1 is an ~550 μm-sized fragment consisting mainly of plagioclase (at least one large single crystal and several smaller laths), with two interstitial areas containing glass and other fine-grained phases (Fig. 3a). The upper (as seen in Fig. 3a) glassy area contains needles of ilmenite, some of which are flanked by dendritic silica (Fig. 3b). The lower glassy area contains small (<20 μm) anhedral grains of pyroxene, and tiny block-shaped grains of silica (Fig. 3c). One large (~125 μm) grain of phosphate occurs along the edge of the upper glass area and several smaller ones occur as inclusions in plagioclase.

Clast 19 (Fig. 3d) is an ~500 μm-sized fragment consisting mainly of glass, which contains needles of ilmenite flanked by dendritic silica, plus three subhedral (~90-125 μm) crystals of pyroxene. By comparison to clast B1 and other albitic clasts, clast 19 appears to be an unusually large sample of mesostasis from the albitic lithology.

Clast 9 (Fig. 3e) is an ~800 μm-sized fragment constaining 2-3 plagioclase phenocrysts, with groundmass consisting of smaller plagioclase laths, skeletal to dendritic pyroxenes and ilmenite, and small glassy mesostasis areas. It contains seven phosphate grains that are ~30-100 μm in size, as well as several smaller ones. It also contains one ~100 μm-sized grain of ilmenite. Clast 20 (Fig. 3f) is an ~300 μm-sized fragment consisting mainly of groundmass material similar to that in clast 9, with one larger area of plagioclase and one ~125 μm-sized phosphate grain.

Compositions of plagioclase in clast B1 range from $An_{9.1}Or_{3.0}$ to $An_{1.4}Or_{5.8}$ (Table 1) and are among the most albitic observed in this lithology (Fig. 2b). Compositions of plagioclase in clasts 9 ($An_{10.3}Or_{2.7}$ to $An_{0.7}Or_{7.1}$) and 20 ($An_{5.8}Or_{3.5}$ to $An_{0.7}Or_{6.8}$) are in the same range (Fig. 2b). Pyroxenes in clast B1 and clast 9 (all small grains in the groundmass) have intermediate Fe/Mg ratios (~0.55-0.78) relative to the entire population of albitic clasts, with a wide range of Wo values from ~9 to 50 (Fig. 1, 2). The 3 larger pyroxene grains in clast 19 are among the most ferroan observed for the albitic lithology (Fe/Mg ~1.3-2.1), with intermediate Wo values of ~13-20 (Fig. 1,2). No pyroxenes in clast 20 were large enough to yield good analyses. Glasses in clast B1 and clast 19 (Table 1), as well

as glassy mesostasis areas of clasts 9 and 20, have high concentrations of FeO (Fe/Mg ~15-20), TiO_2 (~1-2 wt.%), K_2O (~3-4 wt.%) and P_2O_5 (up to ~2 wt.%). MnO values are in the range ~0.10-0.55 wt.% and Cr_2O_3 values are below the EMPA detection limit. All glass compositions together form well-defined trends of decreasing P_2O_5, Na_2O, CaO, FeO and MnO with increasing SiO_2, and increasing K_2O and Al_2O_3 with increasing SiO_2 (Supplemental Material), consistent with fractional crystallization. TiO_2 contents in the glasses are variable (Supplemental Material) and locally related to the presence or absence of ilmenite. Phosphates include both apatite and whitlockite (Table 1).

3.2. ^{53}Mn-^{53}Cr Results

The Mn-Cr isotope data from olivine, pyroxene, ilmenite, phosphate, and glass are shown in Table 2. The $^{55}Mn/^{52}Cr$ ratios are high and quite variable (500-58,000) in glass, showing correlated ^{53}Cr excesses of up to ~1,500‰ in DaG 165 clast 19 (Fig. 4a). These data clearly show evidence of live ^{53}Mn at the time of formation of these clasts. The slope of the correlation line obtained from the well-correlated isochron plot for clast 19 corresponds to $(^{53}Mn/^{55}Mn)= (2.84\pm0.10)\times10^{-6}$ (2σ). The initial Cr isotope ratio of the isochron is slightly negative, $(^{53}Cr/^{52}Cr)=-4.2\pm1.0$‰. This negative value may be due to unknown analytical bias in the ion microprobe; however, the effect is negligibly small compared to the large excess ^{53}Cr in glass, so that the initial Cr isotope ratio does not change the slope of the isochron significantly. Although Shukolyukov and Lugmair (2006) identified a negative $^{54}Cr/^{52}Cr$ isotope anomaly in ureilites, our analyses do not use $^{54}Cr/^{52}Cr$ ratio for mass fractionation correction because instrumental mass fractionation is again small compared to the large excess of ^{53}Cr in glass. Compared to the LEW 86010 angrite, with initial $(^{53}Mn/^{55}Mn)= (1.25\pm0.07)\times10^{-6}$ (Lugmair and Shukolyukov, 1998), DaG 165 clast 19 is 4.38±0.18 Ma older, corresponding to the absolute age of 4562.93±0.24 Ma. If we use the D'Orbigny angrite with initial $(^{53}Mn/^{55}Mn)= (3.24\pm0.04)\times10^{-6}$ (Glavin et al., 2004), which is now accepted as a more reliable age anchor (Wadhwa et al., 2009), DaG 165 clast 19 is 0.70±0.18 Ma younger, corresponding to the absolute age of 4563.72±0.22 Ma. A similar absolute age of 4563.85±0.24 Ma is calculated using another angrite, NWA 4801, as age anchor (Shukolyukov et al. 2009; Amelin and Irving, 2007).

The Mn-Cr data from glass in DaG 319 clast B1 also plot along the same isochron (Fig. 4b). Regression of an isochron using only the clast B1 data gives the indistinguishable initial ratio of $(^{53}Mn/^{55}Mn)= (2.6\pm1.7)\times10^{-6}$ (2σ).

Phosphate analyses from two other clasts, DaG 165 clast 9 and clast 20, show relatively high ($^{55}Mn/^{52}Cr$) ratios of ~200 and also plot along the clast 19 isochron (albeit with large analytical uncertainties).

3.3. ^{26}Al-^{26}Mg Results

The Al-Mg isotope data from pyroxene and plagioclase in DaG 319 clast B1 are shown in Table 3 and Fig. 5. The $^{27}Al/^{24}Mg$ ratio of plagioclase is fairly constant at ~900 and the data show resolvable ^{26}Mg excesses of ~2‰. Data from three laboratories collected with 3 different SIMS instruments (ims-3f, -6f and -1270) agree well with each other. The slope of the isochron defined by the pyroxene and plagioclase data is $(3.0\pm1.1)\times10^{-7}$ (2σ), corresponding to a time difference of 5.4 (-0.3/+0.5) Ma after CAI compared to the value $(4.96\pm0.25)\times10^{-5}$ from type B CAI AJEF in the Allende CV chondrite (Jacobsen et al., 2008). Using the absolute Pb-Pb age of the same CAI (Jacobsen et al., 2008), the absolute age of DaG 319 clast B1 is estimated to be 4562.2 (+0.5/-0.6) Ma. Compared to the D'Orbigny angrite with initial $^{26}Al/^{27}Al=(5.06\pm0.92)\times10^{-7}$ (Spivak-Birndorf et al., 2009), DaG 319 clast B1 is 0.5 (-0.3/+0.5) Ma younger, and yields an absolute age of 4563.9 (+0.4/-0.5) Ma. This is in agreement with the ^{53}Mn-^{53}Cr age (relative to D'Orbigny) from clast 19, but is 1.7±1 Ma older than the absolute age estimated from the CAI anchor. This discrepancy could be caused by the absolute Pb-Pb age obtained for AJEF (4567.60±0.36Ma). Bouvier and Wadhwa (2009) reported an older (by ~1 Ma) Pb-Pb age of 4568.67±0.17 Ma for a type B CAI in NWA 2364 (CV3). Nevertheless, both CAIs show indistinguishable initial $^{26}Al/^{27}Al$ ratios of $\sim5\times10^{-5}$ (Jacobsen et al., 2008; Bouvier and Wadhwa, 2009). Thus, although there are clearly unresolved issues in the absolute Pb-Pb ages of CAIs, the relative ^{26}Al age of DaG 319 clast B1, ~5.4 Ma after CAI, is not affected. Citing an average of the clast 19 ^{53}Mn-^{53}Cr age and the clast B1 $^{26}Al/^{27}Al$ age, both calculated relative to D'Orbigny, our best estimate of the absolute age of the feldspathic lithology in polymict ureilites is 4563.8±0.4 Ma.

4. Discussion

4.1. Concordance of Al-Mg and Mn-Cr systems and comparison to other differentiated meteorites

In Fig. 6, we plot initial $^{26}Al/^{27}Al$ of DaG 319 Clast B1 and $^{53}Mn/^{55}Mn$ ratios of DaG 165 Clast 19, compared to these ratios in other old achondrites, specifically the D'Orbigny angrite and Asuka 881394 basaltic meteorite (Glavin et al., 2004; Spivak-Birndorf et al., 2009; Wadhwa et al., 2009). These samples plot consistently on a single $^{26}Al/^{27}Al$ –$^{53}Mn/^{55}Mn$ growth line. Since our isotope data were obtained from glass and albitic plagioclase, which

could be easily disturbed by subsolidus thermal processes, the concordance of the obtained $^{26}Al/^{27}Al$ and $^{53}Mn/^{55}Mn$ age dates suggests that they preserved their primary isotope record after solidification. Furthermore, the DaG 165 and DaG 319 clasts we studied show oxygen isotope ratios consistent with those of main group ureilites (Kita et al., 2006), so it is clear that they are derived from a parent body distinct from the parent bodies of angrites and basaltic achondrites. The $^{26}Al/^{27}Al$ – $^{53}Mn/^{55}Mn$ growth line corresponds to a $^{53}Mn/^{55}Mn$ ratio of $\sim 8\times10^{-6}$ at the time of CAI formation, assuming an initial $^{26}Al/^{27}Al$ ratio of 5×10^{-5} (MacPherson et al., 1995).

Our results for ^{26}Al-^{26}Mg and ^{53}Mn-^{53}Cr isotopes of several clasts from the albitic lithology in polymict ureilites (Table 4) indicate a crystallization age ~0.5 Ma younger than that of the oldest angrites, D'Orbigny and Sahara 99555 (Glavin et al., 2004; Spivak-Birndorf et al., 2009), ~2 Ma younger than that of the Asuka 881394 basaltic meteorite (Wadhwa et al., 2009), and at least 1 Ma younger than that of the oldest non-cumulate eucrite, Chervony Kut (Lugmair and Shukolyukov, 1998, 2001). In the following section we discuss implications of this crystallization age for differentiation of the ureilite parent body (UPB).

4.2. Implications for differentiation of the ureilite parent body

The obtained age of 4563.8±0.4 Ma (relative to D'Orbigny), or ~5.4 Ma after CAI (Table 4), is consistent with the most precise previous age data for both main group and polymict ureilites, including the Pb-Pb age of MET 78008 (Torigoye-Kita et al., 1995b), the Pb-Pb age of an apatite grain in DaG 319 (Kita et al., 2002), and previous Al-Mg data for plagioclase in DaG 319 (Kita et al., 2003). In addition, we suggest that the Mn-Cr data of Shukolyukov and Lugmair (2006) for Kenna and LEW 85440 may be consistent with our results. Although Shukolyukov and Lugmair (2006) argued that Cr isotopes in these main group ureilites equilibrated after all ^{53}Mn had decayed, this conclusion was based on a dataset that included Mn-enriched leachates. These leachates may have contained olivine rim material, which is known to have elevated Mn/Cr ratios (compared to olivine core compositions) due to late shock-melting and/or reduction processes (Goodrich et al., 1987). Eliminating these leachates leaves a dataset (residues and whole rock analyses) that is consistent with the DaG 165 isochron (Fig. 4), albeit with large uncertainties.

Three models have been considered to explain an age of ~5 Ma after CAI for both main group ureilites and the albitic lithology in polymict ureilites. Here we summarize and evaluate these models.

Model 1: Kita et al. (2005) considered a simple model for internal heating of the UPB by decay of ^{26}Al and ^{60}Fe. This work showed that if the UPB (compositionally similar to anhydrous CI chondrites) accreted at ~2.3-2.5 Ma after CAI, then the parental melt of the feldspathic clasts could have been generated at ~5.2 Ma after CAI by 10-20% silicate melting at a peak temperature of ~1150˚C. This temperature is similar to equilibration temperatures of the most ferroan main group ureilites, .but falls short of those (up to ~1300°C) required for the most magnesian (e.g. Takeda, 1989; Singletary and Grove, 2003). Thus, Kita et al. (2005) postulated that additional heat was provided by the melt itself, migrating toward the surface of the parent body and concentrating the heat source (dominantly ^{26}Al) in shallower source regions. This would lead to a reverse temperature gradient on the UPB, with the highest temperatures near the surface and lower temperatures at depth, consistent with smelting (Singletary and Grove, 2003). This model predicts that the final equilibration temperatures of main group ureilites were attained at ~9 Ma after CAI. Although Kita et al. (2005) not directly address the thermal history of the feldspathic clasts (i.e. the products of the melts), it is extremely unlikely that their Al-Mg and Mn-Cr isotopic systems could have closed at ~5.4 Ma after CAI, given this much longer cooling history for their host body.

Model 2: An alternative model discussed by Kita et al. (2005) is that the age of ~5 Ma after CAI for the feldpathic clasts is the time of impact disruption of the UPB. In this model, the UPB accreted at 2.2 Ma and silicate partial melt was generated and migrated toward the surface at 4.7 Ma. At 5.2 Ma after CAI, the UPB reached temperatures ranging from 1200 to 1300˚C, and at this point was disrupted by impact. The feldspathic clasts may represent melts that were solidified during the subsequent rapid cooling of ejected material. Both ultramafic residual material and selected feldspathic components could then have accreted to a new parent body from which current ureilitic meteorites are derived (e.g. Goodrich et al., 2004).

This model has the strong point that quenching of melt to form the feldspathic clasts during impact ejection would quickly close their Al-Mg and Mn-Cr isotopic systems. However, it is not clear whether it can explain the petrologic characteristics of these clasts. Assuming that their parent melt was basaltic, extensive fractionation processes are require to explain their mineral and chemical compositions. For example, Cohen et al. (2004) calculated that >90% fractional crystallization was required to reach the high Fe/Mg ratios of pyroxenes in DaG 165 clast 19, given a parent melt related to main group ureilites, and Kita et al. (2004) reached a similar conclusion based on trace elements in plagioclase. Such high degrees of fractionation are unlikely to occur during impact ejection and quenching of melt from high temperatures.

Model 3: Wilson et al. (2008) developed a detailed model that tracked heating due to the decay of radioisotopes, melting, and melt migration on the UPB as a function of formation time and other initial conditions. Although 17 short-lived radionuclides were included in this model, the thermal history was controlled almost entirely by ^{26}Al, with a small contribution (slightly increasing as melting proceded) from ^{60}Fe. The basic constraints, derived from the smelting model of Goodrich et al. (2007), were peak temperatures of ~1250°C in the shallowest source regions (3 MPa) and ~1150°C in the deepest (10 MPa). Results showed that the UPB (compositionally similar to CV chondrites) must have accreted at ~0.55 Ma after CAI, with silicate melting beginning at ~1 Ma after CAI. The initial melt production rate was extremely high, such that ~half of total silicate melting occurred in a very short time around 1 Ma after CAI and all basaltic melts were produced during this period. At first glance, this result appears to be grossly inconsistent with the ~5.4 Ma after CAI age obtained in this work for the most abundant feldspathic lithology in polymict ureilites. However, Wilson et al. (2008) also showed that ~15% of the melt produced on the UPB was emplaced in shallow intrusions (which as in model 1 are instrumental in achieving the highest temperatures in the shallowest source regions), and argued that these intrusions are the source of the indigenous feldspathic material in polymict ureilites.

Based on calculated cooling histories for these intrusions, this model is consistent with the highly fractionated petrologic and chemical characteristics of the albitic lithology (e.g. reaching crystallization temperatures <1000°C at ~5 Ma after CAI), and with requirements for a minimum of chemical and isotopic exchange between the melt and the wall rock (Goodrich et al., 2007; Wilson et al., 2008). It is also consistent with the requirement for closure of the Al-Mg and Mn-Cr isotopic systems at ~5.4 Ma after CAI, based on the 950 K (~677°C) Mn-Cr closure temperature. inferred from olivine in Rumuruti chondrules by Sugiura and Miyazaki (2006). However, other studies have suggested that diffusion of Mg in plagioclase (at least anorthite) and Cr in olivine can be very fast at temperatures much lower than 677°C (LaTourrette and Wasserburg, 1998; Grossman and Brearley, 2005). Given the subsequent slow cooling history predicted for these intrusions (Wilson et al., 2008), their Al-Mg and Mn-Cr isotopic systems may not have remained closed. Another possibility, however, is that the feldspathic clasts represent melt that was erupted during intermittent explosive eruptions from the intrusions (Wilson et al., 2008) after extensive fractionation. Such a model could satisfy both the petrologic and isotopic constraints.

Re-cap: Any model to explain an age of ~5.4 Ma after CAI for the albitic lithology in polymict ureilites must satisfy both the petrologic constraints (high degree of igneous fractionation relative to basaltic melt) and the isotopic

constraints (closure of the Al-Mg and Mn-Cr isotopic systems). Of the 3 models that have been proposed, model 1 fails to satisfy the isotopic constraints. Model 2 offers a promising mechanism for quenching the isotopic systems, but requires further work to determine whether it is consistent with the petrologic constraints. Model 3 explains the petrologic characteristics of the clasts but requires further work to determine whether it can meet the constraints of isotopic closure. All 3 models are consistent with the best absolute ages obtained for main group ureilites (i.e. the residues of the partial melting that led to these clasts), but because even the most precise of these ages (e.g. 4563±6; Torigoye-Kita et al., 1995b) has large errors compared to the data obtained here, they do not provide a strong constraint. In addition, a further constraint on any thermal model for the UPB is the abundant evidence that main group ureilites have experienced a two-stage cooling history (Mittlefehldt et al., 1998) – slow cooling at high temperatures in the range ~1275-1100°C, followed by rapid cooling on the order of 3-20°C/hr through the range ~1000-600°C (e.g. Goodrich et al., 2001; Mori and Takeda, 1983; Toyoda et al., 1986). This extreme change in cooling rate is commonly interpreted as a result of impact disruption of the parent body while still hot (Mittlefehldt et al., 1998). Model 2 clearly accounts for this event. However, model 3 can also accommodate impact disruption of a hot UPB at any time in the interval from ~5-9 Ma after CAI. Finally, we note that models 2 and 3 differ significantly in terms of inferred time of accretion and start of silicate melting. This difference is primarily due to the assumption of batch melt extraction in model 2 (Kita et al., 2005) versus fractional melt extraction in model 3 (Wilson et al., 2008). Although Wilson et al. (2008) based the assumption of fractional melting on physical modelling of melt migration rates and mode, studies of the feldspathic materials in polymict ureilites have yet to show unambiguously whether they are products of fractional or batch melting (Kita et al., 2004; Cohen et al., 2004). We emphasize that the petrogenesis of the highly-evolved albitic clasts, and their relationship to main group ureilites, is not well understood (Cohen et al., 2004; Kita et al., 2004). The age data obtained in this work, and the evidence for preservation of concordant Al-Mg and Mn-Cr isotopic compositions in plagioclase and glass, provide important new constraints on their origin and a mimimum age for the differentiation of the ureilite parent asteroid.

5. Conclusions

Mn-Cr and Al-Mg isotopic data from several clasts belonging to the most abundant population of feldspathic materials in polymict ureilites show correlated ^{53}Cr and ^{26}Mg excesses clearly indicating the presence of live ^{53}Mn and ^{26}Al at the time of formation. Initial $^{26}Al/^{27}Al$ and $^{53}Mn/^{55}Mn$ ratios obtained from these data plot on a single

growth line with the D'Orbigny angrite and the Asuka 881394 eucrite, and yield an age of 4563.8 Ma (anchored to D'Orbigny), or ~5.4 Ma after CAI. Interpretation of this age for the differentiation history of the ureilite parent body depends on a number of currently model-dependent parameters, such as size, bulk composition and oxygen fugacity, as well as the petrologic relationship of the feldspathic clasts to main group ureilites. Further modeling is required to explain both the highly fractionated petrologic characteristics of the feldspathic clasts and the closure of their Al-Mg and Mn-Cr isotopic systems at ~5.4 Ma after CAI.

Acknowledgements

We thank Sasha Krot for suggesting that we analyze ^{53}Mn-^{53}Cr in polymict ureilites, and Günter Lugmair and Harold Connolly for helpful discussions about ureilite and early solar system chronology. We thank Kent Ross for assistance with EMPA,Yuichi Morishita and Gen Shimoda for their support on the GSJ SIMS work, and Jennifer Matzel and Benjamin Jacobsen for assistance with the Mn-Cr relative sensitivity factor measurements. We greatly appreciate the comments and criticisms of reviewers Alexander Shukolyukov and Joel Baker, and the Editor Richard Carlson, which led to significant improvements in this manuscript. This work was supported by NASA grants NAG5-1191 and NNX08AE08G to Klaus Keil, NNG05GH72G and NNX08AG63G to Cyrena Goodrich, NNX07AI46G to Noriko Kita, NNH07AG01I to Ian Hutcheon, and NAG5-8158 to Gary Huss. This work performed under the auspices of the U.S. Department of Energy by Lawrence Livermore National Laboratory under Contract DE-AC52-07NA27344.

References

Amelin, Y., 2008a. U-Pb ages of angrites. Geochim. Cosmochim. Acta 72, 221-232.

Amelin, Y., 2008b. The U-Pb systematics of angrite Sahara 99555. Geochim. Cosmochim. Acta 72, 4874-4885.

Amelin Y., Irving A. J., 2007. Seven million years of evolution on the angrite parent body from Pb-isotopic data. Workshop on the chronology of meteorites and the early solar system, LPI Contribution No. 1374. pp. 20–21.

Amelin, Y., Krot, A.N., Hutcheon, I.D., Ulyanov, A.A., 2002. Lead isotopic ages of chondrules and calcium-aluminum-rich inclusions. Science 297, 1678-1683.

Amelin, Y. Connelly, J., Zartman, R.E., Chen, J.H., Göpel, C., Neymark, L.A., 2009. Modern U-Pb chronometry of meteorites: advancing to higher time resolution reveals new problems. Geochim. Cosmochim. Acta 73, 5212-5223.

Armstrong, J. T., Huneke, J. C., Shaw, H. F., Finnerty, T. A., Wasserburg, G. J., 1982. Standard $CaAl_2Si_2O_8$ glasses with various Mg isotopic compositions for ion microprobe characterization, in: Heinrich, K.F.J. (Ed.), Microbeam Analysis—1982. San Francisco Press, pp. 205-209.

Baker, J., Bizzarro, M., Wittig, N., Connelly, J., Haack, H., 2005. Early planetesimal melting from an age of 4.5662 Gy for differentiated meteorites. Nature 436, 1127-1131.

Berkley, J.L., Brown, H.G., Keil, K., Carter, N.L., Mercier, J-C.C., 1976. The Kenna ureilite: an ultramafic rock with evidence for igneous, metamorphic, and shock origin. Geochim. Cosmochim. Acta 40, 1429-1437.

Berkley, J.L.,Taylor, G.J., Keil, K., Harlow, G.E., Prinz M., 1980. The nature and origin of ureilites. Geochim. Cosmochim. Acta 44, 1579-1597.

Berkley, J.L., Jones, J.H., 1982. Primary igneous carbon in ureilites: petrological implications. Proc. Lunar Planet. Sci. Conf. 13, A353-A364.

Bouvier, A., Wadhwa, M., 2009. Synchronizing the absolute and relative clocks: Pb-Pb and Al-Mg systematics in CAIs from the Allende and NWA 2364 CV3 chondrites. Lunar Planet. Sci. 40, #2184.

Boynton, W.V., Starzyk, P.M., Schmitt, R.A., 1976. Chemical evidence for the genesis of the ureilites, the achondrite Chassigny and the nakhlites. Geochim. Cosmochim. Acta 40, 1439-1447.

Catanzaro, E. J. Murphy T. J. Garner E. L., Shields W. R., 1966. Absolute isotopic abundance ratios and atomic weight of magnesium. J. Res. Nat. Bur. Stand. 70A, 453-458.

Clayton, R.N., Mayeda, T.K., 1988. Formation of ureilites by nebular processes. Geochim. Cosmochim. Acta 52, 1313-1318.

Clayton, R.N., Mayeda, T.K., 1996. Oxygen-isotope studies of achondrites. Geochim. Cosmochim. Acta 60, 1919-2018.

Cohen, B.A., Goodrich, C.A., Keil, K., 2004. Feldspathic clast populations in polymict ureilites: stalking the missing basalts from the ureilite parent body. Geochim. Cosmochim. Acta 68, 4249-4266.

Davis, A.M, Prinz, M., Laughlin, J.R., 1988. An ion-microprobe study of plagioclase-rich clasts in the North Haig polymict ureilite. Lunar Planet. Sci. 19, 251-252.

Downes, H., Mittlefehldt, D.W., Kita, N.T., Valley, J.W., 2008. Evidence from polymict ureilites for a disrupted and re-accreted single ureilite parent asteroid gardened by several distinct impactors. Geochim. Cosmochim. Acta, 72, 4825-4844.

Fahey, A. J., Goswami, J.N., McKeegan, K. D., Zinner, E. K, 1987. ^{26}Al, ^{244}Pu, ^{50}Ti, REE, and trace element abundances in hibonite grains from CM and CV meteorites. Geochim. Cosmochim. Acta 51, 329-350.

Glavin, D.P., Kubny, A., Jagoutz, E., Lugmair, G.W., 2004. Mn-Cr isotope systematics of the D'Orbigny angrite. Meteorit. Planet. Sci. 39, 693-700.

Goodrich, C.A., 1992. Ureilites: A critical review. Meteoritics 27, 327-352.

Goodrich, C.A., 1999. Are ureilites residues from partial melting of chondritic material? The answer from MAGPOX. Meteorit. Planet. Sci. 34, 109-119.

Goodrich, C.A., Delaney, J.S., 2000. Fe/Mg-Fe/Mn relations of meteorites and primary heterogeneity of primitive achondrite parent bodies. Geochim. Cosmochim. Acta 64, 2255-2273.

Goodrich, C.A., Lugmair, G.W., 1995. Stalking the LREE-enriched component in ureilites. Geochim. Cosmochim. Acta 59, 2609-2620.

Goodrich, C.A., Jones, J.H., Berkley, J.L., 1987. Origin and evolution of the ureilite parent magmas: multi-stage igneous activity on a large parent body. Geochim. Cosmochim. Acta 51, 2255-2273.

Goodrich, C.A., Patchett, P.J., Lugmair, G.W., Drake, M.J., 1991. Sm-Nd and Rb-Sr isotopic systematics of ureilites. Geochim. Cosmochim. Acta 55, 829-848.

Goodrich, C.A., Lugmair, G.W., Drake, M.J., Patchett, P.J., 1995. Comment on "U-Th-Pb and Sm-Nd isotopic systematics of the Goalpara ureilite: resolution of terrestrial contamination" by N. Torigoye-Kita, K. Misawa, and M. Tatsumoto. Geochim. Cosmochim. Acta 59, 4083-4085.

Goodrich, C.A., Fioretti, A.M., Tribaudino, M., Molin, G., 2001. Primary trapped melt inclusions in olivine in the olivine-augite-orthopyroxene ureilite Hughes 009. Geochim. Cosmochim. Acta 65, 621-652.

Goodrich, C.A., Hutcheon, I.D., Keil, K., 2002. ^{53}Mn-^{53}Cr age of a highly-evolved, igneous lithology in polymict ureilite DaG 165. Meteorit. Planet. Sci. 37, A54.

Goodrich, C.A., Scott, E.R.D., Fioretti, A.M., 2004. Ureilitic breccias: clues to the petrologic structure and impact disruption of the ureilite parent asteroid. Chemie de Erde 64, 283-327.

Goodrich, C.A., Van Orman, J., Wilson, L., 2007. Fractional melting and smelting on the ureilite parent body. Geochim. Cosmochim. Acta 71, 2876-2895.

Grossman, J.N., Brearley, A.J., 2005. The onset of metamorphism in ordinary and carbonaceous chondrites. Meteorit. Planet. Sci. 40, 87-122.

Guan, Y., Crozaz, G., 1995. The quest for the elusive LREE carrier in ureilites: an ion microprobe study. Lunar Planet. Sci. 26, 527-528.

Göbel, R., Ott, U., Begemann, F., 1978. On trapped noble gases in ureilites. J. Geophys. Res. 83, 855–867.

Ikeda, Y., Prinz, M., 2001. Magmatic inclusions and felsic clasts in the Dar al Gani 319 polymict ureilite. Meteorit. Planet. Sci. 36, 481-499.

Ikeda, Y., Prinz, M., Nehru, C.E., 2000. Lithic and mineral clasts in the Dar al Gani (DaG) 319 polymict ureilite. Antarctic Meteorite Research 13, 177-221.

Jacobsen, B., Yin, Q.-Z., Moynier, F., Amelin, Y., Krot, A. N., Nagashima, K., Hutcheon, I. D., Palme, H., 2008. ^{26}Al–^{26}Mg and ^{207}Pb–^{206}Pb systematics of Allende CAIs: Canonical solar initial ^{26}Al/^{27}Al ratio reinstated. Earth Planet Sci. Lett. 272, 353-364.

Keil, K., Wilson, L., 1993. Explosive volcanism and the compositions of cores of differentiated asteroids. Earth Planet. Sci. Lett. 117, 111-124.

Kita, N.T., Nagahara, H., Togashi, S. , Morishita, Y., 2000. A short duration of chondrule formation in the solar nebula: evidence from ^{26}Al in Semarkona ferromagnesian chondrules. Geochim. Cosmochim. Acta 64, 3913-3922.

Kita, N.T., Ikeda, Y., Morishita Y., 2002. The old Pb-Pb age of apatite in felsic clast of polymict ureilite DaG 319. Meteorit. Planet. Sci. 37, A79.

Kita, N.T., Ikeda, Y., Shimoda, H., Morishita, Y., Togashi, S., 2003. Timing of basaltic volcanism in ureilite parent body inferred from the ^{26}Al ages of plagioclase-bearing clasts in DaG 319 polymict ureilite. Lunar Planet Sci. 34, #1557.

Kita, N.T., Ikeda, Y., Togashi, S., Liu, Y., Morishita, Y., Weisberg, M.K., 2004. Origin of ureilites inferred from a SIMS oxygen isotopic and trace element study of clasts in the Dar al Gani 319 polymict ureilite. Geochim. Cosmochim. Acta 68, 4213-4235.

Kita, N.T., Ikeda, Y., Shimoda, G., Togashi, S., Morishita, Y., Weisberg, M.K., 2005. Internal heating of the ureilite parent body by short-lived nuclides. Meteorit. Planet. Sci. 40, 5178.

Kita, N.T., Goodrich, C.A., Fu, B., Spicuzza, M.J.,Valley, J.W., 2006. Oxygen isotopes in mafic and feldspathic clasts from polymict ureilites. Meteorit. Planet. Sci. 41, A96.

Kita, N.T., Hutcheon, I.D., Huss, G.R., Goodrich, C.A., 2007. ^{26}Al-^{26}Mg and ^{53}Mn-^{53}Cr age of a feldspathic lithology in polymict ureilites. Meteorit. Planet. Sci. 42, 5231.

LaTourrette, T., Wasserburg, G.J., 1998. Mg diffusion in anorthite: implications for the formation of early solar system planetesimals. Earth Planet. Sci. Lett. 158, 91-108.

Lee, D-C., Halliday, A.N., Singletary, S.J., Grove, T.L., 2003. ^{182}Hf-^{182}W chronometry for an early differentiation in the parent body of ureilites. Lunar Planet. Sci. 34, #1179.

Lee, D-C., Halliday, A.N., Singletary, S.J., Grove, T.L., 2005. ^{182}Hf-^{182}W chronometry and an early differentiation in the parent body of ureilites. Lunar Planet. Sci. 36, #1638.

Lugmair, G.W., Galer, S.J.G., 1992. Age and isotopic relationships among angrites Lewis Cliff 86010 and Angra dos Reis. Geochim. Cosmochim. Acta 56, 1673-1694.

Lugmair, G.W., Shukolyukov, A., 1998. Early solar system timescales according to ^{53}Mn-^{53}Cr systematics. Geochim. Cosmochim. Acta 62, 2863-2886.

Lugmair, G.W., Shukolyukov, A., 2001. Early solar system events and timescales. Meteorit. Planet. Sci. 36, 1017-1026.

MacPherson G. J., Davis A. M., Zinner E. K., 1995. The distribution of aluminum-26 in the early solar system: a reappraisal. Meteoritics 30, 365–386.

Matzel, J., Jacobsen, B., Hutcheon, I., Kita, N., Ryerson, F., 2009. Influence of bulk chemical composition on relative sensitivity factors for $^{55}Mn/^{52}Cr$ by SIMS: Implications for the ^{53}Mn-^{53}Cr chronometer. AGU, Fall Meeting, ID#V33E-06.

McKeegan, K. D., Walker, R. M., Zinner, E. K., 1985. Ion microprobe isotopic measurements of individual interplanetary dust particles. Geochim. Cosmochim. Acta 49, 1971-1987.

McKibbin, S.J., Avila, J.N., Ireland, T.R., Holden, P., St. C. O'Neill, H., 2008. Isotopic compositions and systematics of early solar system and presolar materials: an evaluation of matrix effects and mass interferences. Meteorit. Planet. Sci. 43, Suppl., #5149.

Mittlefehldt, D.W., 1986. Fe-Mg-Mn relations of ureilite olivines and pyroxenes and the genesis of ureilites. Geochim. Cosmochim. Acta 50, 107-110.

Mittlefehldt, D.W., McCoy, T.J., Goodrich, C.A., Kracher, A., 1998. Non-chondritic meteorites from asteroidal bodies, in: Papike, J.J. (Ed.), Planetary Materials, Reviews in Mineralogy 36. Mineralogical Society of America., pp. 4-1 to 4-195.

Mittlefehldt, D.W., Hudon, P., Galindo, C., Jr., 2005. Petrology, geochemistry and genesis of ureilites. Lunar Planet. Sci. 36, #1140.

Mori, H., Takeda H., 1983. An electron petrographic study of ureilite pyroxenes. *Meteoritics* **18**, 358-359.

Nehru, C.E., Weisberg, M.K., Prinz, M., 1997. Chromites from three primitive achondrite groups. Meteorit. Planet. Sci. 32, A97.

Prinz, M., Weisberg, M.K., Nehru, C.E., 1988. Feldspathic components in polymict ureilites. Lunar Planet. Sci. 19, 947-948.

Rankenburg, K., Brandon, A.D., Humayun, M., 2007. Osmium isotope systematics of ureilites. Geochim. Cosmochim. Acta 71, 2402-2413.

Scott, E.R.D., Taylor, G.J., Keil K., 1993. Origin of ureilite meteorites and implications for planetary accretion. Geophys. Res. Lett. 20, 415-418.

Shukolyukov, A., Lugmair, G. W., 2006. The Mn–Cr isotope systematics in the ureilites Kenna and LEW 85440. Lunar Planet. Sci. 37, #1478..

Shukolyukov, A., Lugmair, G.W., Irving A. J., 2009. Mn – Cr isotope systematics of angrite Northwest Africa 4801. Lunar Planet. Sci. 40, #1381.

Singletary, S.J., Grove, T.L., 2003. Early petrologic processes on the ureilite parent body. Meteorit. Planet. Sci. 38, 95-108.

Sinha, S.K., Sack, R.O., Lipschutz, M.E., 1997. Ureilite meteorites: equilibration temperatures and smelting reactions. Geochim. Cosmochim. Acta 61, 4325-4242.

Spitz, A.H., Boynton, W.V., 1991. Trace element analysis of ureilites: new constraints on their petrogenesis. Geochim. Cosmochim. Acta 55, 3417-3430.

Spitz, A.H., Goodrich, C.A., Crozaz, G., Lundberg, L., 1988. Ion microprobe search for the LREE host phase in ureilite meteorites. Lunar Planet. Sci. 19, 1111-1112.

Spivak-Birndorf, L., Wadhwa, M., Janney P., 2009. ^{26}Al-^{26}Mg systematics in D'Orbigny and Sahara 99555 angrites: implications for high-resolution chronology using extinct chronometers. Geochim. Cosmochim. Acta 73, 5202-5211.

Sugirua, N., Miyazaki, A., 2006. Mn-Cr ages of Fe-rich olivine in two Rumuruti (R) chondrites. Earth Planets Space 58, 689-694.

Sugiura, N., Ichimura, K., Fujiya, W., Takahata, N., Sano, Y., 2009. A preliminary study on ^{55}Mn/^{52}Cr relative sensitivity for a synthetic calcite: implications. Meteorit. Planet. Sci. 44, Suppl., #5316.

Takahashi, K., Masuda, A., 1990. The Rb-Sr and Sm-Nd dating and REE measurements of ureilites. Meteoritics 25, 413.

Takeda, H., 1989. Mineralogy of coexisting pyroxenes in magnesian ureilites and their formation conditions. Earth Planet. Sci. Lett. 93, 181-194.

Tatsumoto, M., Knight, T.J., Allègre, C.J., 1973. Time differences in the formation of meteorites as determined by ^{207}Pb/^{206}Pb. Science 180, 1279-1283.

Torigoye-Kita, N., Misawa, K., Tatsumoto, M., 1995a. U-Th-Pb and Sm-Nd isotopic systematics of the Goalpara ureilite: resolution of terrestrial contamination. Geochim. Cosmochim. Acta 59, 381-390.

Torigoye-Kita, N., Tatsumoto, M., Meeker, G.P., Yanai, K., 1995b. The 4.56 Ga U-Pb age of the MET 78008 ureilite. Geochim. Cosmochim. Acta 59, 2319-2329.

Torigoye-Kita, N., Misawa, K., Tatsumoto, M., 1995c. Reply to the Comment by C.A. Goodrich, G.W. Lugmair, M.J. Drake, and P.J. Patchett on "U-Th-Pb and Sm-Nd isotopic systematics of the Goalpara ureilite: resolution of terrestrial contamination." Geochim. Cosmochim. Acta 59, 4087-4091.

Toyoda, H., Haga, N., Tachikawa, O., Takeda, H., Ishii T., 1986. Thermal history of ureilite, Pecora Escarpment 82506 deduced from cation distribution and diffusion profile of minerals. Proceedings of 10th Symposium on Antarctic Meteorites, 206–221.

Van Orman, J.A., Goodrich, C.A., Wilson, L., 2009. Metal and siderophile elements in ureilites: reconciliation with smelting? Lunar Planet Sci. 40, #1986.

Wadhwa, M., Srinivasan, G., Carlson, R.W., 2006. Timescales of planetesimal differentiation in the early solar system, in: Lauretta, D.S., McSween, H.Y., Jr. (Eds.), Meteorites in the the Early Solar System II. University of Arizona, Tucson. pp. 715-731.

Wadhwa, M., Amelin, Y., Bogdanovski, O., Shukolyukov, A., Lugmair, G.W., Janney, P., 2009. Ancient relative and absolute ages for a basaltic meteorite: implications for timescales of planetesimal accretion and differentiation. Geochim. Cosmochim. Acta 73, 5189-5201.

Walker, D., Grove, T.L., 1993. Ureilite smelting. Meteoritics 28, 629-636.

Warren, P.H., Huber, H., 2006. Ureilite petrogenesis: a limited role for smelting during anatexis and catastrophic disruption. Meteorit. Planet. Sci. 41, 835-849.

Warren, P.H., Kallemeyn, G.W., 1992. Explosive volcanism and the graphite-oxygen fugacity buffer on the parent asteroid(s) of the ureilite meteorites. Icarus 100, 110-126.

Warren P.H., Ulff-Moeller F., Huber H. and Kallemeyn G.W., 2006. Siderophile geochemistry of ureilites: a record of early stages of planetesimal core formation. Geochim. Cosmochim. Acta 70, 2104-2126.

Wasserburg, G.J., Tera, F., Papanastassiou, D.A., Huneke, J.C., 1977. Isotopic and chemical investigations on Angra dos Reis. Earth Planet. Sci. Lett. 35, 294-316.

Weisberg, M.K., McCoy, T.J., Krot, A.N., 2006. Systematics and evaluation of meteorite classification, in: Lauretta, D.S., McSween, H.Y., Jr. (Eds.), Meteorites in the the Early Solar System II. University of Arizona, Tucson. pp. 20-52.

Wilson, L.W., Goodrich, C.A., Van Orman, J.A., 2008. Thermal evolution and physics of melt extraction on the ureilite parent body. Geochim. Cosmochim. Acta 72, 6154-6176..

FIGURE CAPTIONS

Fig. 1. Compositions of pyroxenes in DaG 319 clast B1 and DaG 165 clasts 19 and 9, compared to entire population of albitic clasts in polymict ureilites DaG 164/165/319 and EET 83309 (Cohen et al., 2004).

Fig. 2. (a) Molar Fe/Mg vs. Fe/Mn in pyroxenes in DaG 319 clast B1 and DaG 165 clasts 19 and 9, compared to entire population of albitic clasts in DaG 164/165/319 and EET 83309 (Cohen et al., 2004). Albitic lithology shows a normal igneous fractionation trend; this is in contrast to main group ureilites, which show a nearly pure redox trend (Goodrich et al., 1987). (b) Anorthite content (An) of plagioclase vs. molar Fe/Mg of pyroxenes in DaG 319 clast B1 and DaG 165 clast 9, compared to entire population of albitic clasts in DaG 164/165/319 and EET 83309 (Cohen et al., 2004). Error bars represent the range of observed compositions within each clast. Fractional crystallization trend was calculated for a melt that begins crystallization near the low-Fe/Mg, high-An data points on the diagram, and does not correspond to a particular petrogenetic model for the albitic lithology.

Fig. 3. Back-scattered electron images (BEI) of clasts analyzed in this study. (a) DaG 319 clast B1, outlined in black. Clast consists dominantly of plagioclase (plag). Two glassy intergranular areas, outlined by white boxes, are shown at higher magnification in [b] and [c]. (b) Upper glass (gl) area of clast B1. Glass contains thin needles of ilmenite (white), flanked by tiny grains of dendritic silica (dark). Note that glass is also crosscut by veins of terrestrial iron oxides, which are also white but distinguished from the ilmenite by being thicker and curved. Large light grey grain on right is phosphate (ph). (c) Lower glass (gl) area of clast B1. Anhedral, light grey grains are pyroxenes (px). Small, dark, block-shaped grains in glass are silica. (d) DaG 165 clast 19, consisting dominantly of glass (gl) with needles of ilmenite (white) flanked by dendritic silica (dark). Larger, subhedral grains (light grey) are pyroxene (px). Pits in glass and pyroxene are from ^{53}Mn-^{53}Cr analysis. (e) Portion of DaG 165 clast 9, outlined in white (full clast is shown in Fig. 2a of Cohen et al., 2004). Clast consists of a few large plagioclase grains and intersertal-textured groundmass of smaller plagioclase laths, skeletal and dendritic pyroxenes and ilmenite (light grey and white), and glassy mesostatis. This portion of the clast also contains 7 rounded grains of phosphate (ph); pit in one labelled grain is from ^{53}Mn-^{53}Cr analysis. (f) Portion of DaG 165 clast 20, consisting mainly of groundmass similar to that in clast 9. Pit in large grain of phosphate (ph) is from ^{53}Mn-^{53}Cr analysis. Black area on right is edge of section.

Fig. 4. ^{53}Mn-^{53}Cr isochron diagrams for polymict ureilite clasts. Data are from Table 2. (a) DaG 165 clast 19 (open circles). ^{55}Mn/^{52}Cr ratios in FeO-rich glass are as high as 60,000, with extremely high ^{53}Cr excess up to 1,500‰. The slope of the isochron corresponds to the ^{53}Mn/^{55}Mn ratio of $(2.84\pm0.10)\times10^{-6}$. The absolute age is calculated to be 4563.72±0.22 Ma using the D'Orbigny angrite age anchor. (b) Data for DaG 165 clasts 9 (open diamonds), clast 20 (open triangles) and DaG 319 clast B1 (filled squares). Data for clast 19 are also shown. The regression of an isochron from clast B1 indicates the initial ^{53}Mn/^{55}Mn ratio of $(2.6\pm1.7)\times10^{-6}$ in agreement of clast 19 within error. Insert shows phosphates, olivine, pyroxene and ilmenite data, which plot on the isochron of clast 19 near the origin.

Fig. 5. ^{26}Al-^{26}Mg isochron diagram for DaG 319 clast B1. Data are from Table 3. Circles and squares indicate data from plagioclase and pyroxene. The slope of the isochron corresponds to the ^{26}Al/^{27}Al ratio of $(3.0\pm1.1)\times10^{-7}$. The absolute ages are calculated to be 4562.2+0.5/-0.6 Ma and 4563.9+0.4/-0.5 Ma using the Allende AJEF CAI and D'Orbigny angrite age anchors, respectively.

Fig. 6. The relative ages of achondrites indicated from short-lived nuclides ^{26}Al and ^{53}Mn. The inferred ^{26}Al/^{27}Al of DaG 319 clast B1 and ^{53}Mn/^{55}Mn ratios of DaG 165 clast 19 (this work) are compared to those of the Asuka 881394 basaltic meteorite (Wadhwa et al., 2009) and D'Orbigny angrite (Glavin et al., 2004; Spivak-Birndorf et al. 2009). The line indicates decay of the ^{26}Al/^{27}Al and ^{53}Mn/^{55}Mn ratios with time after CAI (with the initial ^{26}Al/^{27}Al ratio of 5×10^{-5}; MacPherson et al., 1995) that passes through age anchor D'Orbigny. Three achondrites plot on a consistent decay line.

Supplemental Material Figure. Compositions of glass in DaG 165 clast 19 and two glass areas of DaG 319 clast B1. The three glasses show well-defined trends for most elements vs. SiO_2 (an index of fractionation). One analysis of glassy mesostasis in DaG 165 clast 20 also plots along these trends. Glassy mesostasis areas in DaG 165 clast 9 shows a similar composition, but are too small for quantitative electron microprobe analysis.

Table 1. Electron microprobe analyses of glasses, phosphates and plagioclase in clasts from polymict ureilites DaG 319 and DaG 165.

	Clast B1 upper[a] glass avg. (8)	Clast B1 lower[a] glass avg. (5)	Clast 19 glass avg. (13)	Clast B1 whit.[b] avg. (2)	Clast 9 apatite avg. (5)	Clast 9 whit. avg. (3)	Clast 20 apatite avg. (3)	Clast B1 plag	Clast B1 plag	Clast B1 plag	Clast B1 plag
SiO_2	69.2 ± *1.3*	71.7 ± *0.9*	66.9 ± *0.9*	0.09	0.50	0.61	0.49	64.9	66.4	66.4	67.6
TiO_2	1.29 ± *0.51*	2.08 ± *0.55*	1.22 ± *0.14*	bdl	na	na	na	0.13	0.12	0.18	0.17
Al_2O_3	7.11 ± *0.60*	10.1 ± *1.83*	5.98 ± *0.51*	bdl	0.04	0.10	0.04	21.4	21.2	20.4	20.1
Cr_2O_3	bdl	bdl	bdl	bdl	bdl	bdl	bdl	bdl	bdl	bdl	bdl
FeO	12.2 ± *1.56*	7.50 ± *2.67*	14.9 ± *1.12*	1.85	1.59	1.72	2.37	0.35	0.25	0.42	0.80
MgO	0.53 ± *0.13*	0.31 ± *0.11*	0.48 ± *0.07*	3.12	0.28	3.06	0.36	bdl	bdl	bdl	bdl
MnO	0.35 ± *0.09*	0.20 ± *0.07*	0.42 ± *0.07*	0.15	0.25	0.12	0.23	bdl	bdl	bdl	bdl
CaO	0.60 ± *0.19*	0.28 ± *0.14*	0.80 ± *0.07*	46.1	52.8	46.4	52.4	1.95	1.25	0.70	0.29
K_2O	3.18 ± *0.14*	3.61 ± *0.34*	2.92 ± *0.17*	2.31	na	na	na	0.54	0.61	0.83	0.99
Na_2O	3.60 ± *0.94*	3.20 ± *0.62*	5.02 ± *0.66*	bdl	0.55	2.47	0.58	10.4	10.4	10.8	10.4
P_2O_5	0.99 ± *0.23*	0.67 ± *0.21*	1.49 ± *0.29*	46.5	41.5	45.8	40.7	na	na	na	na
Cl	na	na	na	bdl	2.67	bdl	2.85	na	na	na	na
Total	99.1 ± *1.4*	99.7 ± *0.8*	100.1 ± *0.6*	100.1	100.2	100.3	100.0	99.7	100.2	99.8	100.4
An								9.1	6.0	3.3	1.4
Or								3.0	3.5	4.7	5.8
Ab								87.9	90.5	92.0	92.7

[a] The designations of upper and lower glass refer to locations as shown in Fig. 3a.
[b] Whitlockite.
bdl = below detection limit.
na = not analyzed.

Table 2. Mn-Cr isotope analyses of clasts from polymict ureilites DaG 165 and DaG 319.

Clast	Phase	$^{55}Mn/^{52}Cr$[a]	$\delta^{53}Cr$ ‰[a]
DaG 165 matrix	Ol	1.2 ± 0.5	-4.2 ± 2.5
	Ol	1.2 ± 0.5	-4.7 ± 1.9
	Ol	1.3 ± 0.5	-4.3 ± 2.9
	Ol	1.3 ± 0.5	-3.9 ± 1.9
	Ol	0.7 ± 0.5	0.30 ± 1.1
	Ol	0.7 ± 0.5	1.7 ± 1.4
DaG 165 Clast 9	Ilmenite	0.9 ± 0.5	-2.3 ± 1.2
	Phosphate	202.6 ± 4.7	3 ± 29
DaG 165 Clast 19	Px 1	6.9 ± 1.0	-3.7 ± 1.3
	Px 2	9.8 ± 1.0	-4.5 ± 1.7
	Px 3	9.5 ± 1.0	-3.2 ± 3.6
	Gl 1A	2,470 ± 80	61 ± 28
	Gl 1B	57,900 ± 2,700	1,497 ± 42
	Gl 2A	2,913 ± 47	59 ± 23
	Gl 2B	2,080 ± 38	40 ± 23
	Gl 2C	1,664 ± 19	40.2 ± 9.2
	Gl 3A	43,900 ± 2,700	1,086 ± 27
	Gl 3B	6,750 ± 440	159 ± 33
	Gl 10-1	4,070 ± 550	76 ± 12
	Gl-10-2	16,600 ± 900	405 ± 25
DaG 165 Clast 20	Phosphate	181.7 ± 4.3	2 ± 24
DaG 319 Clast B1	Gl 1	506 ± 50	32.2 ± 9.2
	Gl 10A	710 ± 40	24 ± 16
	Gl 10B	950 ± 59	31 ± 18
	Gl 11	2,610 ± 200	85 ± 32

[a] Errors quoted are 2 SE.
Ol=olivine.
Px=pyroxene.
Gl=glass.

Table 3. Al-Mg isotope analyses of clast B1 from polymict ureilite DaG 319.

Phase	Lab	$^{27}Al/^{24}Mg$[a]	$\delta^{26}Mg$ ‰[a]
Px	LLNL	1.0 ± 0.1	0.2 ± 0.5
Px	ASU	0.09 ± 0.02	-0.42 ± 0.54
Plag	LLNL	835 ± 45	2.5 ± 2.0
Plag	ASU	889 ± 45	0.81 ± 1.26
Plag	GSJ	939 ± 61	2.33 ± 1.08
Plag	GSJ	960 ± 44	2.18 ± 1.22

[a] Errors quoted are 2 SE.
Px=pyroxene.
Plag=plagioclase.

Table 4. The absolute age of clasts from polymict ureilites with different age anchors.

System	Age Anchor	Initial ratios/ Age (Ma)	Polymict Ureilite Clast/ Initial Ratio	Age (Ma)	
				Relative	Absolute
^{53}Mn-^{53}Cr	LEW 86010 (angrite)	$(1.25 \pm 0.07)\times10^{-6}$ [1] 4558.55±0.15 [2]	DaG 165 Clast 19 $(2.84\pm0.10)\times10^{-6}$	-4.38 ±0.18	4562.93 ±0.24
	D'Orbigny (angrite)	$(3.24\pm0.04)\times10^{-6}$ [3] 4564.42±0.12 [2]		+0.70 ±0.18	4563.72 ±0.22
	NWA 4801 (angrite)	$(0.96\pm0.04)\times10^{-6}$ [4] 4558.06±0.15 [5]		-5.79 ±0.18	4563.85 ±024
^{26}Al-^{26}Mg	AJEF (CAI)	$(4.96\pm0.25)\times10^{-5}$ [6] 4567.60±0.36 [6]	DaG 319 Clast B1 $(3.0\pm1.1)\times10^{-7}$	+5.4 -0.3/+0.5	4562.2 +0.5/-0.6
	D'Orbigny (angrite)	$(5.06\pm0.92)\times10^{-7}$ [7] 4564.42±0.12 [2]		+0.5 -0.4/+0.5	4563.9 +0.4/-0.5

[1] Lugmair and Shukolyukov (1998). [2] Amelin (2008a). [3] Glavin et al. (2004). [4] Shukolyukov et al. (2009). [5] Amelin and Irving (2007). [6] Jacobsen et al. (2008). [7] Spivak-Birndorf et al. (2009).

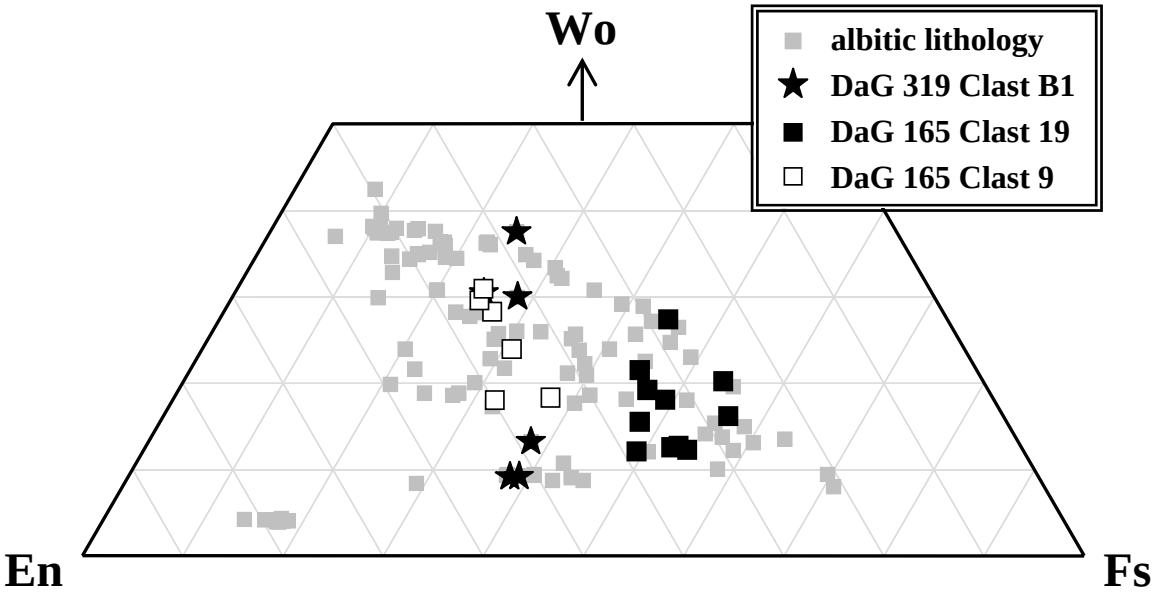
Wo
albitic lithology
DaG 319 Clast B1
DaG 165 Clast 19
DaG 165 Clast 9
En
Fs

Fig. 1

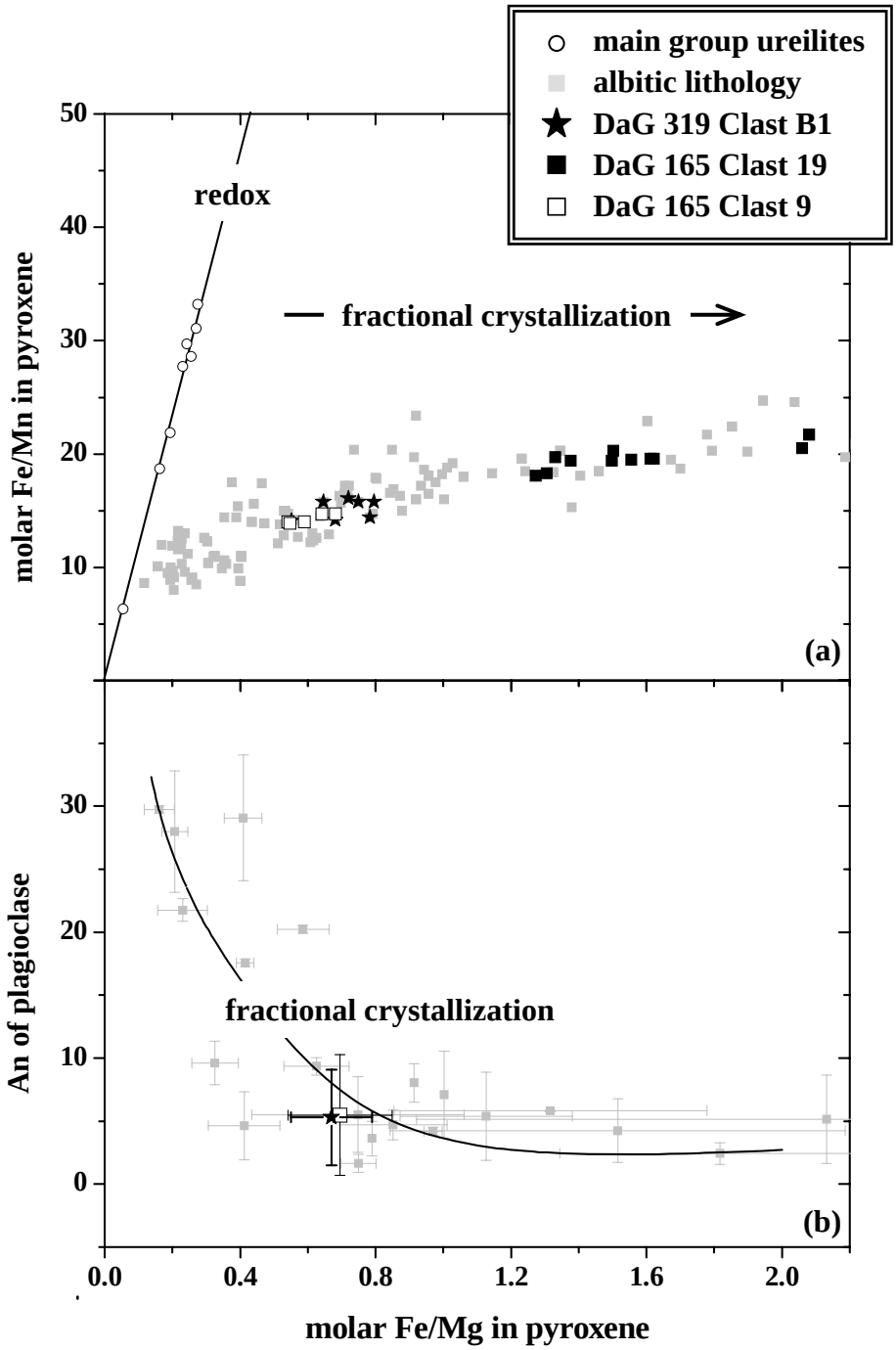
main group ureilites
albitic lithology
DaG 319 Clast B1
DaG 165 Clast 19
DaG 165 Clast 9
redox
fractional crystallization
(a)
fractional crystallization
(b)
molar Fe/Mn in pyroxene
An of plagioclase
molar Fe/Mg in pyroxene
0
10
20
30
40
50
0.0
0.4
0.8
1.2
1.6
2.0

Fig. 2

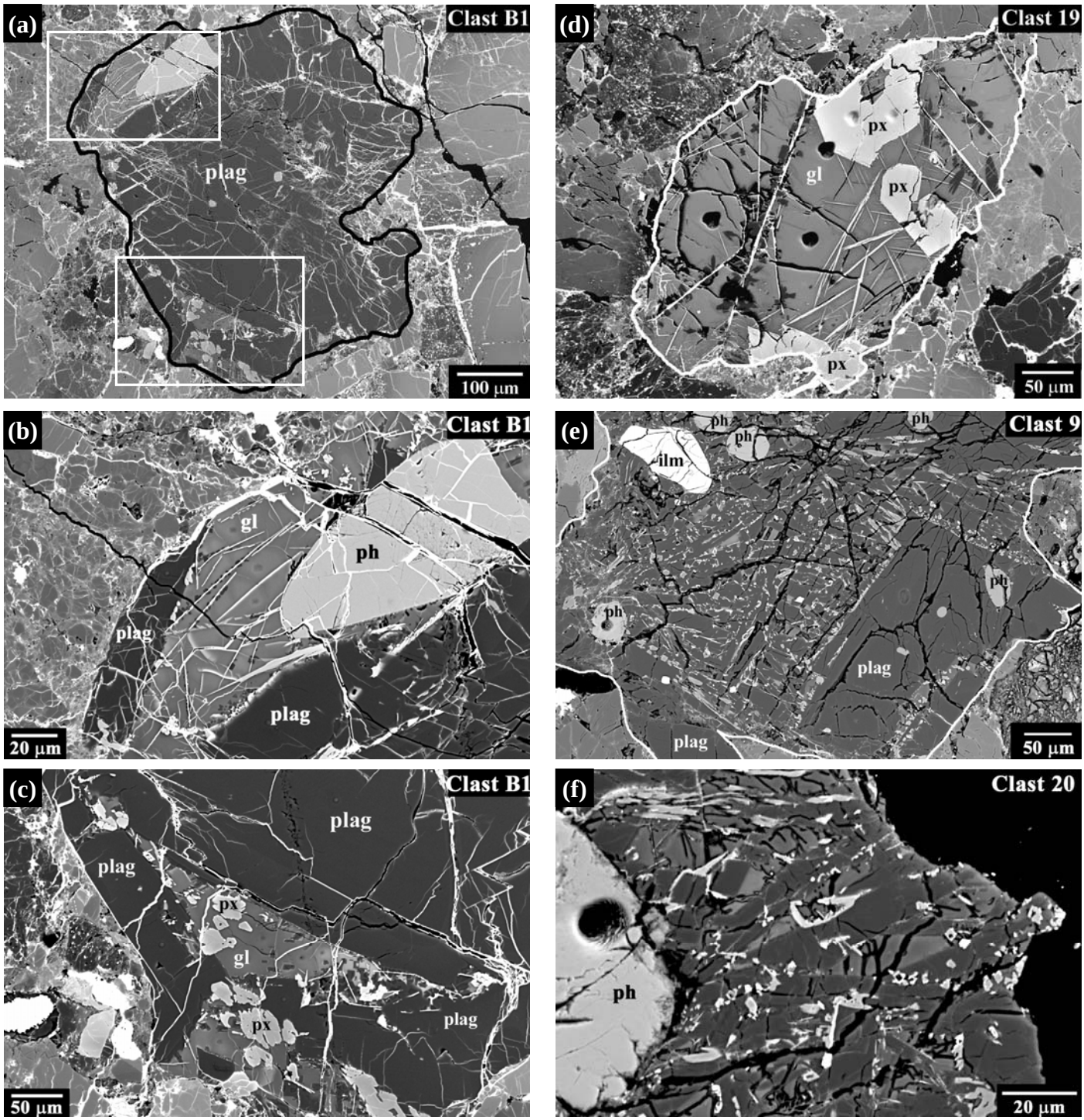
(a)
Clast B1
plag
100 μm
(b)
Clast B1
gl
ph
plag
plag
20 μm
(c)
Clast B1
plag
plag
px
gl
px
plag
50 μm
(d)
Clast 19
px
gl
px
px
50 μm
(e)
Clast 9
ph
ph
ph
ilm
ph
ph
ph
plag
plag
50 μm
(f)
Clast 20
ph
20 μm

Fig. 3

(a)

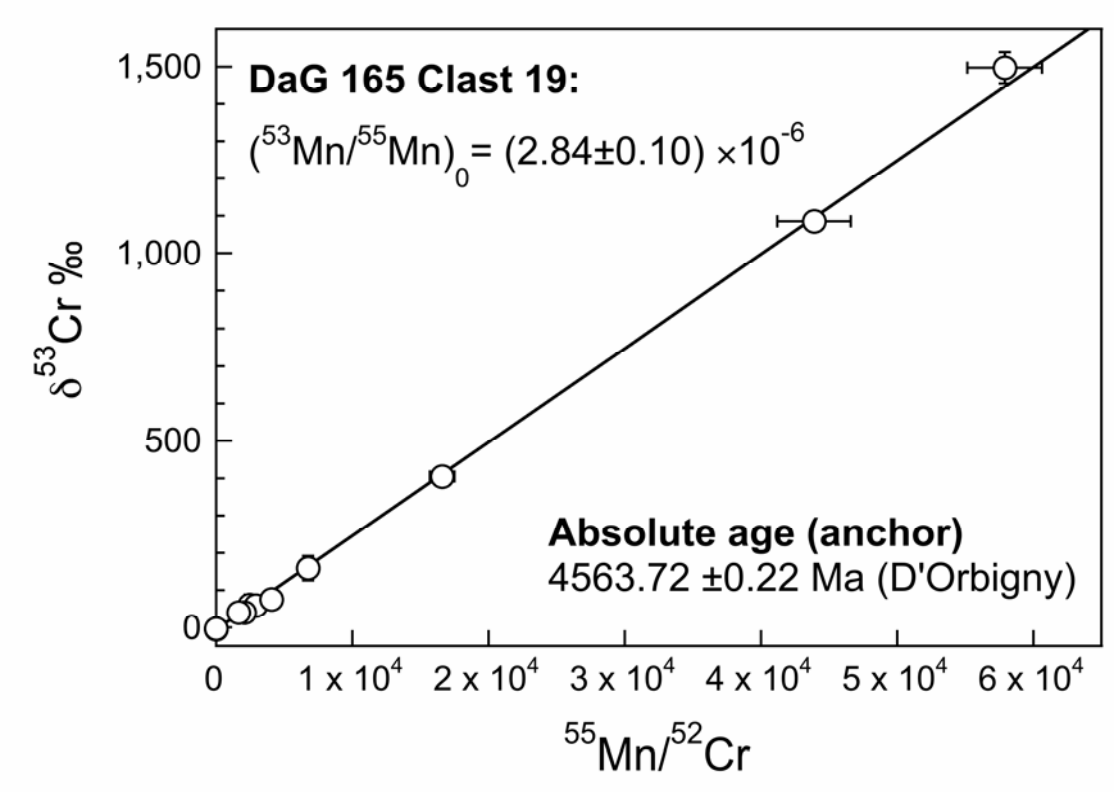
DaG 165 Clast 19:
$(^{53}Mn/^{55}Mn)_0 = (2.84\pm0.10) \times 10^{-6}$
Absolute age (anchor)
4563.72 ±0.22 Ma (D'Orbigny)
$\delta^{53}Cr$ ‰
$^{55}Mn/^{52}Cr$
1,500
1,000
500
0
0
1 x 10^4
2 x 10^4
3 x 10^4
4 x 10^4
5 x 10^4
6 x 10^4

(b)

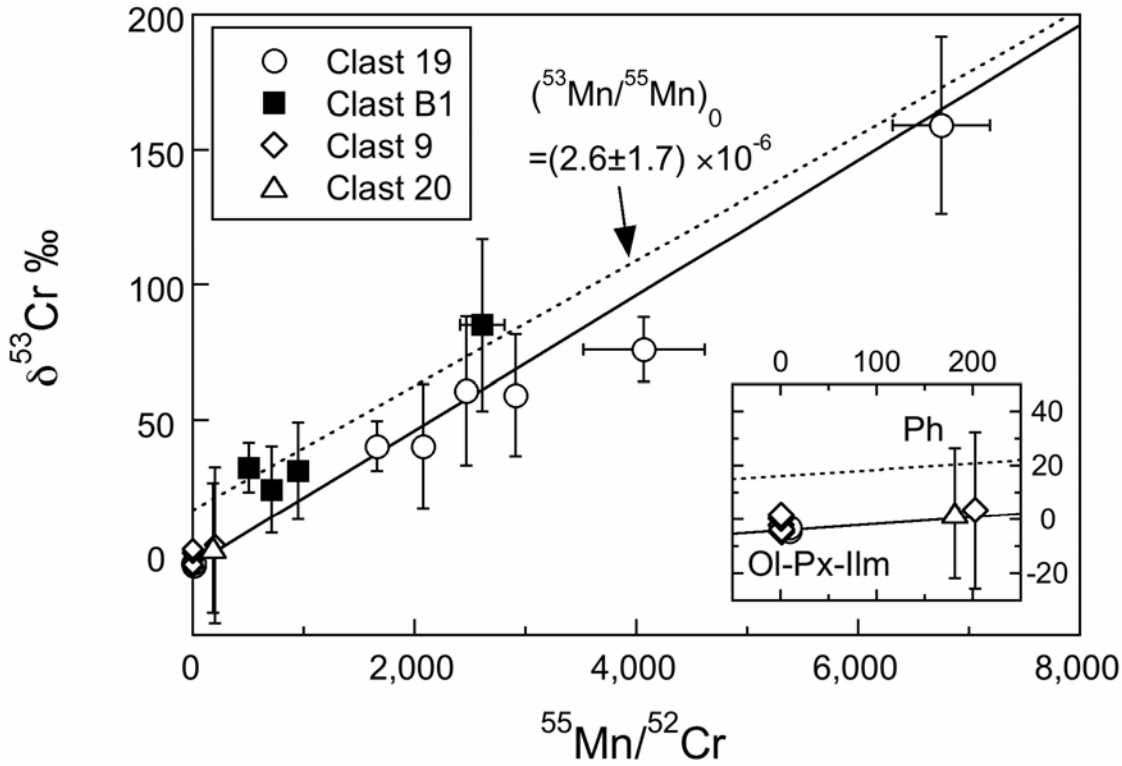
Clast 19
Clast B1
Clast 9
Clast 20
$(^{53}Mn/^{55}Mn)_0$
$=(2.6\pm1.7) \times 10^{-6}$
Ph
Ol-Px-Ilm
$\delta^{53}Cr$ ‰
$^{55}Mn/^{52}Cr$
200
150
100
50
0
0
2,000
4,000
6,000
8,000
0
100
200
40
20
0
-20

Fig. 4

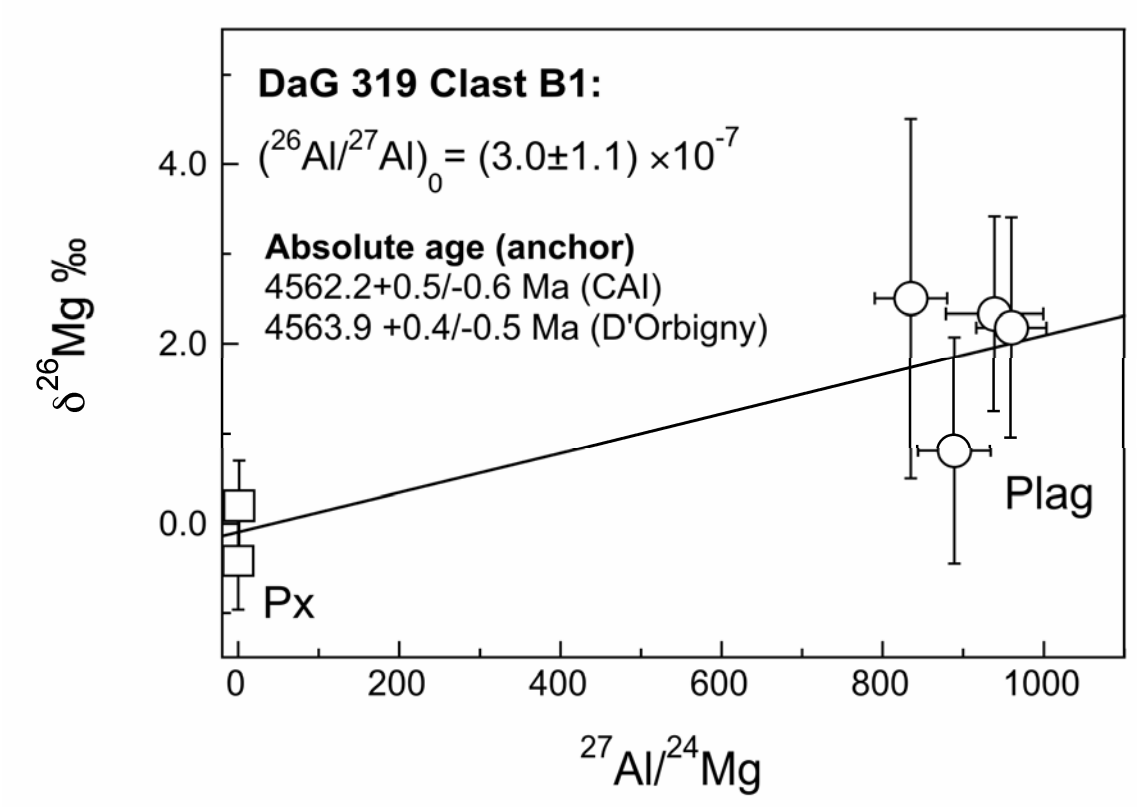
DaG 319 Clast B1:
$(^{26}Al/^{27}Al)_0 = (3.0\pm1.1) \times 10^{-7}$
Absolute age (anchor)
4562.2+0.5/-0.6 Ma (CAI)
4563.9 +0.4/-0.5 Ma (D'Orbigny)
Plag
Px
$\delta^{26}Mg$ ‰
$^{27}Al/^{24}Mg$
4.0
2.0
0.0
0
200
400
600
800
1000

Fig. 5

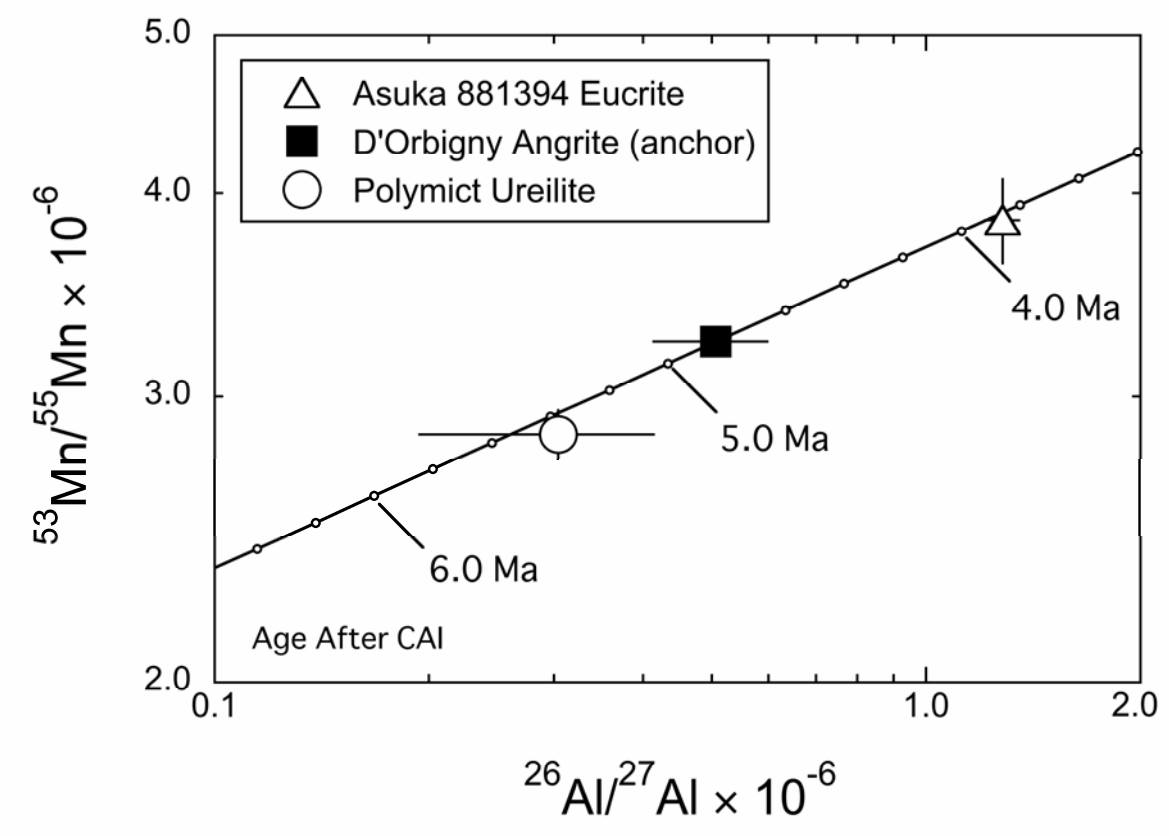
Asuka 881394 Eucrite
D'Orbigny Angrite (anchor)
Polymict Ureilite
4.0 Ma
5.0 Ma
6.0 Ma
Age After CAI
$^{53}Mn/^{55}Mn \times 10^{-6}$
$^{26}Al/^{27}Al \times 10^{-6}$
5.0
4.0
3.0
2.0
0.1
1.0
2.0

Fig. 6

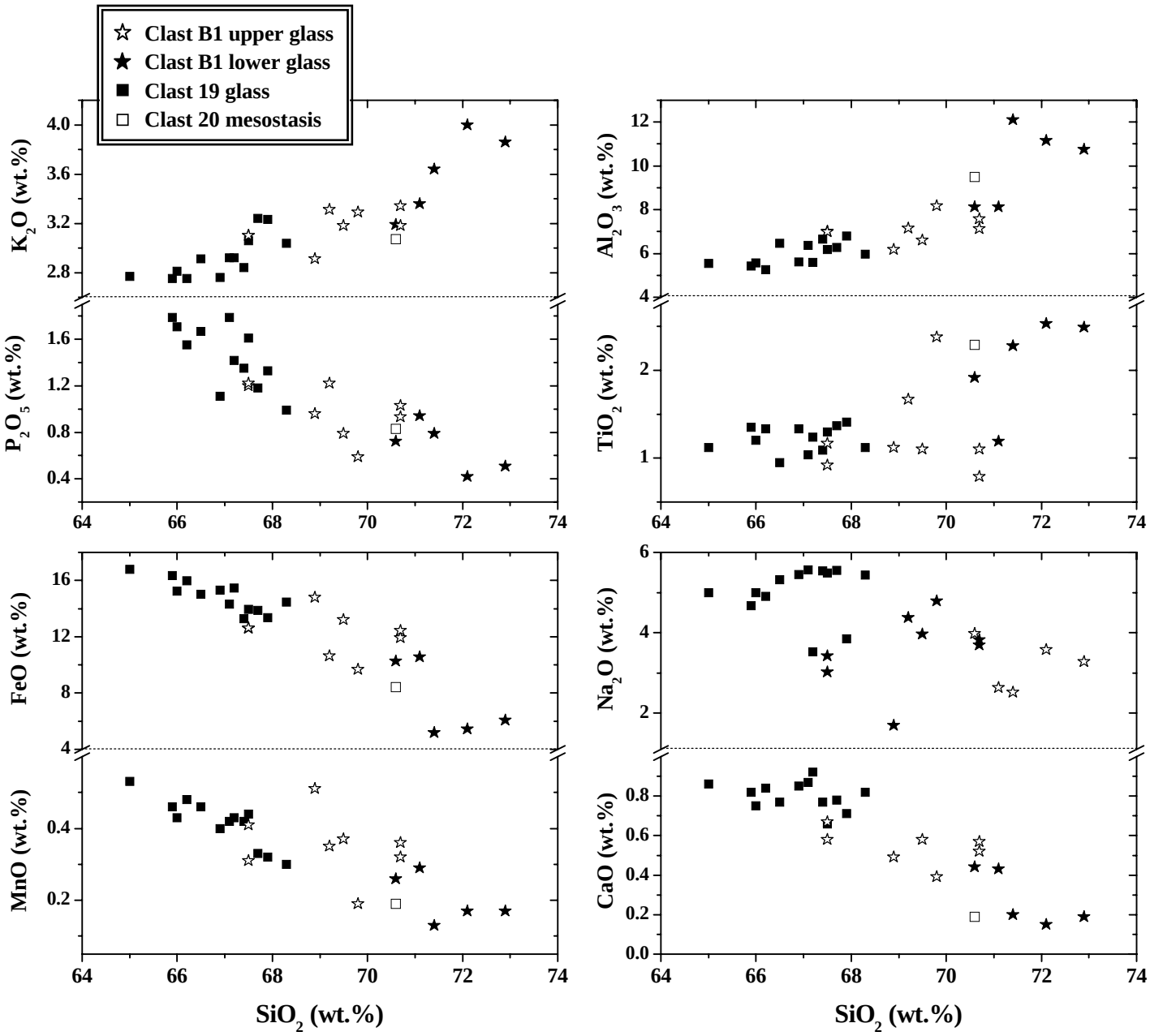

Supplemental Material